OPTICAL CHARACTERIZATION OF DIELECTRIC FILMS ON CURVED SURFACES USING DIFFRACTION METHOD

A Thesis Submitted to
the Graduate School of Engineering and Sciences of
İzmir Institute of Technology
in Partial Fulfillment of the Requirements for the Degree of

MASTER OF SCIENCE

in Electronics and Communication Engineering

by
Çağın EKİCİ

July 2016
İZMİR

We approve the thesis of **Çağın EKİCİ**

Examining Committee Members:

Prof. Dr. Mehmet Salih DİNLEYİCİ
Department of Electrical and Electronics Engineering
İzmir Institute of Technology

Prof. Dr. Emine Yeşim ZORAL
Department of Electrical and Electronics Engineering
Dokuz Eylül University

Assist. Prof. Dr. Kıvılcım Yüksel ALDOĞAN
Department of Electrical and Electronics Engineering
İzmir Institute of Technology

14 July 2016

Prof. Dr. Mehmet Salih DİNLEYİCİ
Supervisor, Department of Electrical and Electronics Engineering
İzmir Institute of Technology

Prof. Dr. Mehmet Salih DİNLEYİCİ
Head of the Department of
Electrical and Electronics Engineering

Prof. Dr. Bilge KARAÇALI
Dean of the Graduate School of
Engineering and Sciences

ACKNOWLEDGMENTS

First of all, I owe a great deal of thanks to my supervisor Prof. Dr. M. Salih Dinleyici for his excellent guidance, tolerance and patience in every stage of my thesis study. Many thanks also for making reasonable amount of time whenever I knocked on his door.

I would like to thank committee members for giving me contribution which helped me a lot in revising the thesis.

I would like to express my sincere thanks to Assist. Prof. Dr. Osman Akın for his supports, helps and favours.

Special thanks to the colleagues and friends from IYTE, namely Göksenin Bozdağ, Başak Esin Güzel, Osman Tayfun Bişkin, Nurhan Arslan, Bilal Orkan Olcay, Aslı Taşçı, Esra Tunçer, Simay Yılmaz, Oktay Karakuş, Azad Karataş, Gizem Soylu, and Yunus Emre Karataş for their helpful suggestions and comments.

Last but definitely not least, I thank my mother Zeynep Ekici and my father Mehmet Ekici a lot for their true and invaluable support. Very special thanks to my brother Dr. Burak Ekici whose motivation and encouragement helped me through some difficult times.

ABSTRACT

OPTICAL CHARACTERIZATION OF DIELECTRIC FILMS ON CURVED SURFACES USING DIFFRACTION METHOD

In this thesis, we aim to characterize optical properties of thin dielectric films coated on curved surfaces. Indeed, optical thin films attract a great deal of attention especially the ones coated on silica based optical waveguides used as sensor system. Therefore, the step index optical fiber is used in the thesis as a substrate due to the fact that the sensor technology tends towards to fiber optic based platforms. In the thesis, a step index optical fiber is coated with polyvinyl alcohol (PVA), then its thickness is mathematically estimated exploiting Fresnel scalar diffraction method. Phase front of the laser light wave comes across with a phase object (fiber optic), transmits through of it and diffracts. Whole process is modeled by using numerical analysis methods and compared to experimental results to obtain desired parameters in MATLAB. The conventional least-squares method is used for comparison purpose.

Although the emphasis is on optical thin film characterization, we demonstrate the application area of diffraction from fiber optic as sensor. It is used to detect adulteration of olive oil that is big concern for the food industry. The refractive index of various mixture of olive oil and sunflower oil is measured with intend to detect adulteration. This feature makes it a good candidate for fiber optic based refractive index sensor and it may bring practicability and precision to the sensing process.

This dissertation gives detailed information about diffraction from fiber optic both theoretically and experimentally. The experiments were realized by using 632.8 nm continuous wave laser. Both of the experimental results demonstrate that phase diffraction method is a powerful technique to characterize optical thin films and to sense refractive index of the surrounding medium.

ÖZET

DİFRAKSİYON YÖNTEMİ KULLANILARAK EĞİMLİ YÜZEYLERDEKİ YALITKAN FİLMLERİN OPTİK KARAKTERİZASYONU

Bu tezde eğimli yüzeylerde optik yalıtkan film kaplamanın karakterizasyonunu amaçlanmıştır. Bu amaçla alt tabakası silikon bazlı optik dalga kılavuzu olan fiber optik kullanılıp, etrafı polivinilalkol film ile kaplanmıştır. Bu durum tamamiyle fiber optik bazlı sensörlerin geliştirilmesine olanak sağlamaktadır. Kaplanan filmin optik karakterizasyonun yapılması için, Fresnel'in difraksiyon teorisinden faydalanılmıştır. Gönderilen dalga yüzleri faz objesiyle karşılaşıp, faz objesi üzerinden geçtikten sonra difraksiyona uğrar. Bütün bu sürecin matematiksel modellenmesi MATLAB programında yapılmıştır. Bu modellemede elde edilen eşitlikler, bazı integral bazlı numerik çözüm tekniklerinden yararlanılarak sonuca ulaştırılmıştır. Yapılan matematiksel modelleme deneyler sonucunda elde edilen difraksiyon deseniyle karşılaştırılıp bulunması istenilen değişkenin tahmin edilmesi hususunda geleneksel en küçük kareler yöntemi kullanılmıştır.

Vurgulamanın asıl olarak kaplanmış fiber optik üzerindeki ince yalıtkan filmlerin karakterizasyonunda olmasının yanısıra, faz difraksiyon yönteminin bir sensör uygulaması olarak yüksek hassasiyetle kırıcılık indisi belirlenmesi, ve buna bağlı olarak zeytinyağındaki tağşiş seviyesi saptanmıştır. Bu bulgular ile difraksiyon yönteminin kırıcılık indisi belirlenmesindeki yüksek hassasiyetli rolü fiber optik bazlı sensör tasarımını mümkün kılabilir.

Yapılan deneylerde 632.8 nm dalga boyunda sürekli dalga çıktısı olan lazer kullanıldı. Sonuç olarak faz difraksiyon yöntemi optik ince filmlerin karakterizasyon ve fiber optik çevresindeki sıvıların kırıcılık indisinin ölçümü amacıyla kullanılabilecek olan güçlü bir method olarak değerlendirilmelidir.

TABLE OF CONTENTS

LIST OF FIGURES viii

LIST OF TABLES xi

LIST OF ABBREVIATIONS xii

CHAPTER 1. INTRODUCTION 1
1.1. Optical Films Coated Fiber Optics 2
1.2. Optical Diffraction 2
1.3. Fiber Optic Sensors 3
1.4. Overview of the Thesis 4

CHAPTER 2. MATHEMATICAL PRELIMINARIES 6
2.1. Mathematical Theory of Diffraction 6
2.1.1. Kirchhoff's Diffraction Theory 6

CHAPTER 3. MATHEMATICAL MODEL FOR PHASE DIFFRACTION 13
3.1. Diffraction From Phase Objects 13
3.1.1. Theoretical Approach 14
3.1.1.1. Diffraction from Fiber Optic 14
3.1.1.2. Diffraction From Three Layer Phase Object 18
3.1.2. Numerical Calculations of Equations 20
3.1.2.1. Quadrature Method 20
3.1.2.2. Fresnel Integrals 22

CHAPTER 4. REFRACTIVE INDEX SENSING 24
4.1. Refractive Index Origins 24
4.2. Surrounding Liquid Medium Refractive Index Sensing 24
4.2.1. Olive Oil Adulteration Detection 25
4.2.2. Experimental Procedure 25
4.2.3. Results 26

CHAPTER 5. OPTICAL DIELECTRIC FILMS ON CURVED SURFACES 31
5.1. Covered Polymer Thickness Sensing 31
5.1.1. Experimental Procedure 32
5.1.2. Results 34

CHAPTER 6. CONCLUSIONS AND FUTURE WORKS 37

REFERENCES 40

APPENDIX A. DERIVATIONS OF THE THEOREM AND THE CONDITION ... 46

LIST OF FIGURES

Figure **Page**

Figure 1.1. Reactive near, Fresnel near and far field demonstration 2

Figure 1.2. Diffraction pattern of transmitted plane wavefronts through coated phase object 3

Figure 2.1. Fresnel's zones 8

Figure 2.2. The domain of integration 9

Figure 2.3. The integeration surfaces 10

Figure 2.4. Illustration of angles to derive Fresnel-Kirchhoff diffraction formula 11

Figure 2.5. Illustrating new boundaries 12

Figure 3.1. (a) Plane wave transmission from optical fiber, (b) Diffraction geometry for optical fiber 14

Figure 3.2. Optical fiber geometry 16

Figure 3.3. (a) Plane wave transmission from coated optical fiber, (b) Diffraction geometry for coated optical fiber 18

Figure 3.4. Cornu's Spiral 23

Figure 4.1. Top view of experimental setup for determining refractive index of the surrounding medium 26

Figure 4.2. Surrounding refractive index determination (distance $\approx$ 4.1 cm) : (a) The dots are normalized experimental intensity distribution, the curve is the theoretical intensity fitted n_s = 1.33198 (b) Diffraction pattern recorded by CCD of a laser beam diffracted by optical fiber surrounded by pure water whose refractive index is 1.33198 27

Figure 4.3. Surrounding refractive index determination (distance $\approx$ 4.1 cm) : (a) The dots are normalized experimental intensity distribution, the curve is the theoretical intensity fitted n_s = 1.46786 (b) Diffraction pattern recorded by CCD of a laser beam diffracted by optical fiber surrounded by pure olive oil whose refractive index is 1.46786 27

Figure 4.4. Surrounding refractive index determination (distance $\approx$ 4.2 cm) : (a) The dots are normalized experimental intensity distribution, the curve is the theoretical intensity fitted n_s = 1.46837 (b) Diffraction pattern recorded by CCD of a laser beam diffracted by optical fiber surrounded by 90% olive oil 10% sunflower oil mixture whose refractive index is 1.46837 28

Figure 4.5. Surrounding refractive index determination (distance $\approx$ 3.6 cm) : (a) The dots are normalized experimental intensity distribution, the curve is the theoretical intensity fitted n_s = 1.47075 (b) Diffraction pattern recorded by CCD of a laser beam diffracted by optical fiber surrounded by 70% olive oil 30% sunflower oil mixture whose refractive index is 1.47075 28
Figure 4.6. Surrounding refractive index determination (distance $\approx$ 4 cm) : (a) The dots are normalized experimental intensity distribution, the curve is the theoretical intensity fitted n_s = 1.47119 (b) Diffraction pattern recorded by CCD of a laser beam diffracted by optical fiber surrounded by 60% olive oil 40% sunflower oil mixture whose refractive index is 1.47119 ... 29
Figure 4.7. Surrounding refractive index determination (distance $\approx$ 4 cm) : (a) The dots are normalized experimental intensity distribution, the curve is the theoretical intensity fitted n_s = 1.47383 (b) Diffraction pattern recorded by CCD of a laser beam diffracted by optical fiber surrounded by pure sunflower oil whose refractive index is 1.47383 29
Figure 4.8. Comparison between the refractometer results, diffraction results, and wavelength dependency adjusted for the refractometer results 30
Figure 5.1. Dip coating process : (a) Immersing fiber optic into PVA solution (b) Withdrawing fiber optic with a constant speed (c) Waiting for solvent to evaporate 33
Figure 5.2. Top view of experimental setup for determining radius of the coated optical fiber 33
Figure 5.3. PVA coated optical fiber 1 : (a) The dots are normalized experimental intensity distribution , the curve is the theoretical intensity fitted c = 62940 nm (b) Diffraction pattern recorded by CCD of a laser beam diffracted by 440 nm PVA coated optical fiber 34
Figure 5.4. PVA coated optical fiber 1 SEM image in BSED mode reveals an overlay thickness of about 508nm 34
Figure 5.5. PVA coated optical fiber 2 : (a) The dots are normalized experimental intensity distribution, the curve is the theoretical intensity fitted c = 63429 nm (b) Diffraction pattern recorded by CCD camera of a laser beam diffracted by 929 nm PVA film coated optical fiber 35

Figure 5.6. PVA coated optical fiber 2 SEM image in BSED mode (a) External view of 970 nm PVA film coated fiber optic (b) Thickness of the overlay is about 970 nm 35
Figure 5.7. PVA coated optical fiber 3 : (a) The dots are normalized experimental intensity distribution, the curve is the theoretical intensity fitted c = 64130 nm (b) Diffraction pattern recorded by CCD camera of a laser beam diffracted by 1630 nm PVA film coated optical fiber 36
Figure 5.8. PVA coated optical fiber 3 SEM image in BSED mode (a) External view of 1670 nm PVA film coated fiber optic (b) Thickness of the overlay is about 1670 nm 36
Figure 6.1. Typical optical fiber sensor coated with adsorbent material 37

LIST OF TABLES

Table **Page**

Table 4.1. Comparison of refractive index values between diffraction based measurements and refractometer based measurements 30

Table 5.1. Summary of Coated Optical Fibers Thicknesses and Errors 36

LIST OF ABBREVIATIONS

BC . . . . . Boundary condition
BSED . . . . . Backscattered electron detector
CCD . . . . . Charge coupled device
DC . . . . . Dip coating
ESA . . . . . Electrostatic self-assembly
FBG . . . . . Fiber bragg gratings
IR . . . . . Infrared
LBT . . . . . Langmuir - Blodgett technique
LPG . . . . . Long-period fiber gratings
PD . . . . . Phase diffraction
PVA . . . . . Polyvinyl alcohol
SPR . . . . . Surface plasmon resonance

CHAPTER 1

INTRODUCTION

Optical thin films have very long history date back to 17^{th} century. The discovery of $Newton's\ Ring$ may be considered as the earliest scientific observation of optical thin films. It can be explained by interference method in a single film with varying thickness. However, at the time, the nature of light was not sufficiently well understood to explain the observations. Once the wave theory of light was accepted after Fresnel's works on diffraction patterns, optical technology started to develop, great progress is still being made. Among large number of optical based technologies, indeed, optical waveguiding is drawn great deal of interests. In 1966 Charles K. Kao published the now famous ground-breaking paper (Kao and Hockham, 1966). Before the Kao's publishment, glass fibers were believed to be improper type of material for guiding light waves due to the high loss from scattering. Kao realized that purification of glass eliminates high signal loss. This pioneering work made fiber optic waveguides important and widely studied subject in both communication and sensor areas.

Fiber optic based sensors bring extra features when they are coated with materials. Fully coated, partially coated, and even multilayer coated fiber optic sensors are widely used. As a coating material, besides dielectric, conductive metal oxides, and metals are utilized. Among these materials, we provide basis for estimation of dielectric films and transparent metal oxides films thicknesses at the wavelength of interest (visible range) by using classical scalar diffraction method. Although it has resolution limit as it is well known, we do not pay it attention since primary target is not resolving 20-30 nm differences. Indeed, utilizing some near field techniques (evanescent fields) one can obtain higher resolution beyond the limits (See Figure 1.1). For diffraction, the classical diffraction integrals can be modified to determine disturbances at reactive near field (Miller, 1991). This modification integral usage might provide higher resolution. Modified integrals are not used in the thesis since evanescent waves as in Fig 1.1 are not taken into account.

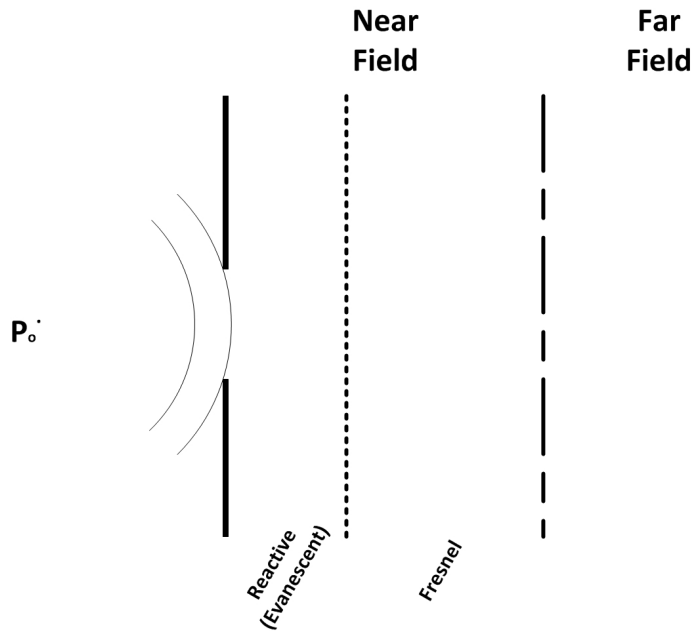

Figure 1.1. Reactive near, Fresnel near and far field demonstration

1.1. Optical Films Coated Fiber Optics

Optical coating films might be described as thin, smooth and parallel to the surface, with thickness varies from few nm to about 20 μm. We also require to thin films to be transparent at the wavelength of interest. These days optical thin films are used everywhere, the range extends from glass anti-reflection coatings to fiber optic based sensors since they are used to improve surface properties. Hence, the characterization of the thin film becomes crucial for any kind of optical components. Here we concentrate basically on optical thin film characterization coated on fiber optic, because we have not come across any kind of powerful technique for that purpose and thin film coated optical fiber sensors have been improved day by day. PVA is used as coating dielectric film due to its low absorption in the visible wavelength, small reflectance, fairly constant refractive index. On the other hand, the work we have done does not introduce restriction for the type of dielectric material. In the experimental point of view, we assume that sending a light through fiber optic which is coated gives reliable results with a screen behind it. Diffraction based methods are appropriate mathematical tool for characterizing thin films on fiber optics, since it turns out to be a method eventually tracing the transmitted wavefront.

1.2. Optical Diffraction

Geometrical optic simply describes light as straight line. According to this treatment, when the light encounters with an opaque body or a slit with a screen behind, the light should illuminate every point on screen except the restrictions that are formed by the body or slit. However, this treatment does not correspond with physical observations. This phenomenon, which violates the law of geometrical optics, is called diffraction or interference in the basic sense. Diffraction effects were proven by asserting light exhibits wavelike behavior. In a similar way electrons exhibit wavelike behavior since electrons diffract as Feynman's experiment pointed out (Feynman et al., 1965).

By definition, diffraction takes place, any region of wavefront is changed sharply in amplitude or phase when light encounters with a slit or a body either transparent or opaque (Hecht, 2002). Although the diffraction phenomena was described more than a century ago, it plays an important role today in many branches of physics and engineering. For instance, classic scalar diffraction from phase object is such a rich subject and its high sensitivity can be taken advantage of estimation coating materials thickness (See Figure 1.2). Moreover, its dependency on surrounding medium properties makes it really good candidate for optical sensor.

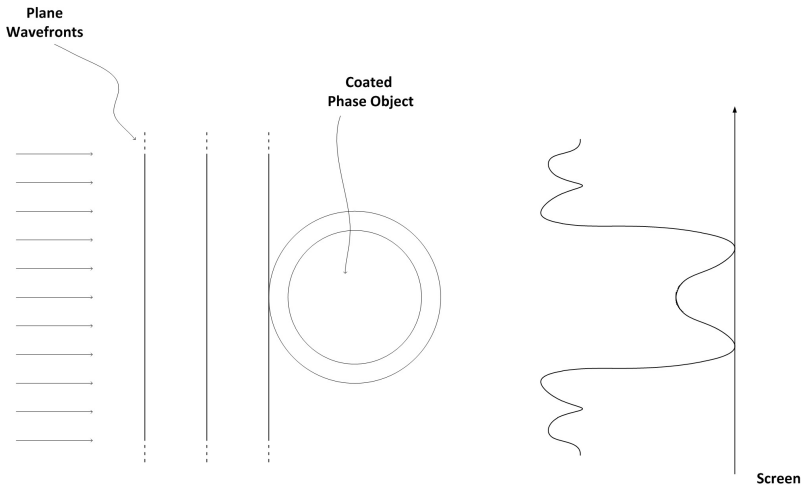

Figure 1.2. Diffraction pattern of transmitted plane wavefronts through coated phase object

1.3. Fiber Optic Sensors

Optical fiber based sensors offer several important inherent advantages over electronic sensors, including low cost, lightweight, immunity to electromagnetic fields, high sensitivity, and high bandwidth. There is no doubt that usage of fiber optic based sensors has increased due to these attractive advantages. Additionally, it brings wealth of application, ranging from medical industry, aerospace industry, through to oil and gas industries. Indeed, fiber optic sensors are the subject of an intense researches and development efforts. Among a large amount of physical and chemical parameters which optical fiber sensors could measure refractive index, temperature, pressure and strain are the most widely studied. Here, we focus on the diffraction based fiber optic sensor to detect adulteration in terms of the refractive index variation of olive oil since adulteration is a big concern for food industry.

1.4. Overview of the Thesis

This thesis is mainly concerned with the phase diffraction (PD) effects and its capability of sensing surrounding medium properties. Primary motivation of the thesis is exploiting Fresnel diffraction method to characterize optical thin films on curved surfaces such as fiber optic. Furthermore, it possible to detect adulteration in the sense of varying refractive index by using same method.

The thesis is organized as follows

Chapter 2 contains a comprehensive discussion of the theory of diffraction by an aperture in a planar opaque screen for the scalar case. The discussion provides a theoretical background for the analysis in the subsequent chapters. It includes a review of Kirchhoff's diffraction theory, its deficiency in terms of the potential theory, and the alternative approaches to this theory.

Chapter 3 examines, in details, mathematical models for the diffraction from both fiber optic and the thin film coated one, numerical calculation of the integral equations.

In Chapter 4, the phase diffraction based sensor is introduced to sense the refractive index of surrounding medium. The sensor is used to detect adulteration of olive oil which is a big concern for food industry for the trial purposes.

In Chapter 5, dip coating procedure is discussed, and the phase diffraction effect is presented to characterize the optical thin films coated on fiber optic. The presented works

and results on this chapter are our main concern.

Finally in the last main Chapter 6, the route of the future works are plotted. Reactive near field resolution, Surface Plasmon Resonance (SPR) based fiber optic sensors and the role of coatings on SPR are discussed.

CHAPTER 2

MATHEMATICAL PRELIMINARIES

In this chapter, we review the derivation of the famous and important scalar diffraction formula which we will use many times in the rest of this dissertation. The theoretical discussion about some diffraction related phenomenons are made. The purpose of this chapter is to reach some conclusions theoretically that might answer the questions about scalar theory of diffraction.

2.1. Mathematical Theory of Diffraction

Theoretical treatment of the diffraction phenomena can be separated into two parts basically : the vectorial (Stratton and Chu, 1939) and the scalar (Theimer et al., 1952). In the field of optics one can generally use scalar approach, but, the more precise treatment is obtained by applying the vectorial approach. In order to transition to the scalar theory, by means of neglecting the vector nature of the light two conditions must be satisfied: (1) Diffraction field must not be calculated at a subwavelength distance from aperture. (2) Diffracting aperture must be large compared with the wavelength of the light (Goodman, 1996). In the scalar approach, polarization of the wave is not taken into account.

The scalar diffraction approach is based on classic Kirchhoff's theory. There are also two other approximations which are widely used; Rayleigh-Sommerfeld theory of first kind which provides the solution to Dirichlet's boundary value problem and Rayleigh-Sommerfeld theory of second kind which provides the solution to Neumann boundary value problem when theory of differential equations analogy is used. Even though the boundary conditions (BC) were defined by the three theories are different, all three often give essentially nearly identical results. They are in very well agreement with experimental observations especially Kirchhoff's theory. Moreover, Kirchhoff's diffraction theory is easy to implement and sufficient to calculate light disturbance at a given point.

2.1.1. Kirchhoff's Diffraction Theory

Treatment of the scalar diffraction theory starts with Huygens' construction. Huygens' intuitive idea asserts that each element of a wavefront may be regarded as the center of a secondary point sources. These point sources produce spherical wavelets whose envelope determine the position of the wavefront at later time (Huygens, 1912). What Fresnel added to the Huygens construction is that postulation of secondary wavelets with the same frequency mutually interfere. This combination is called Huygens-Fresnel Principle. The principle simply describes light propagation. It is expected that light disturbance can be found at an arbitrary point in space provided that phase differences of wavelets are taken into account. Fresnel worked through a spherical monochromatic wavefront which is produced by real point source P_0 and its surface points are regarded as Huygens' virtual point sources (See Figure 2.1). The contribution to the light disturbance $dU(P)$ due to the element dS at Q neglecting time factor $exp(-jwt)$ is (Born and Wolf, 1999)

$$dU(P) \;=\; K(\chi)\, A\, \frac{exp(jkr_0)}{r_0}\, \frac{exp(jks)}{s}\, dS. \tag{2.1}$$

Total disturbance at an arbitrary point P may be found by integrating on the whole surface S

$$U(P) \;=\; A\, \frac{exp(jkr_0)}{r_0} \iint_S \frac{exp(jks)}{s}\, K(\chi)\, dS, \tag{2.2}$$

where A, r_0, and χ represent the amplitude, the radius of the instantaneous position of spherical monochromatic wavefront, and the angle of diffraction, respectively. The inclination factor $K(\chi)$ is introduced to describe the variation of amplitude direction, since contribution of secondary wavelets is not uniform in all direction. This integral is evaluated by dividing spherical wavefront into the number of zones whose radii increase gradually by $\lambda/2$. To a good approximation, inclination factors are nearly equal for the consecutive zones and nearly equal to zero for the larger index zones. Thus, total light disturbance at an arbitrary point P is simply half of the disturbance due to first zone

$$U(P) \;=\; j\,\lambda\, K_1\, \frac{A\, exp(jk(r_0+b))}{r_0+b} = \frac{1}{2}\, U_1(P). \tag{2.3}$$

Kirchhoff examined Huygens-Fresnel principle more rigorously since the inclination factor remained undetermined in the Fresnel's theory. He obtained certain integral theorem for the cases diffraction occurs.

Kirchhoff diffraction formulation basically includes the conversion of the Helmholtz wave equation which is a partial differential equation into certain integral theorem with

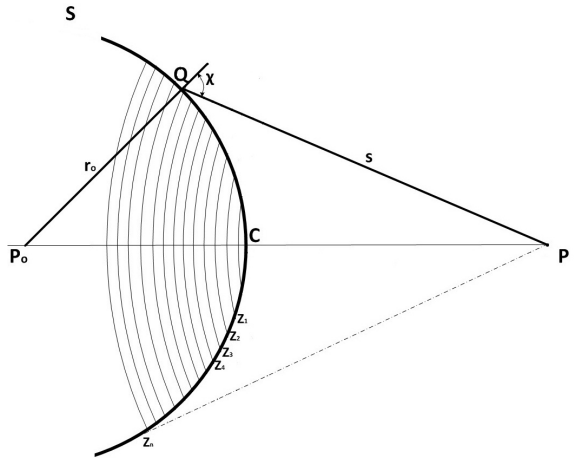

Figure 2.1. Fresnel's zones

the aid of Green's function and Kirchhoff's BC. The mathematical construction of the integral begins with the definition of Green's theorem which helps to find light disturbance U at the observation point in space, might be found in many advanced calculus books.

Let U and G be any two complex-valued position function, and let V be a volume surrounded by closed surface S. If U, G, and their first and second partial derivatives are single-valued and continuous within and on S, then we have

$$\iiint_V (U\nabla^2 G - G\nabla^2 U)\, dV \;=\; \iint_S \left(U\frac{\partial G}{\partial n} - G\frac{\partial U}{\partial n}\right) dS, \tag{2.4}$$

where $\partial/\partial n$ signifies a partial derivative in the outward normal direction at each point on S.

The Equation (2.4) is called Green's theorem. Green's theorem is a consequence of Gauss' theorem. One can easily obtain Green's theorem by choosing two arbitrary scalar functions, using some basic identities and Gauss's theorem. It is the prime foundation of scalar diffraction theory. In order to apply Green's theorem to diffraction one should consider restrictions. These restrictions are appropriate choice of auxiliary Green's function G and closed surface S as boundary. It is clear that U satisfies Helmholtz wave equation. Kirchhoff thought if auxiliary function G also satisfies Helmholtz wave equation, it might be a clever choice since in that case left hand side of Equation (2.4) becomes zero. It reduces the equation much simpler form;

$$(\nabla^2 + k^2)\begin{pmatrix} U \\ G \end{pmatrix} \;=\; 0. \tag{2.5}$$

Therefore, it is easily seen that Equation (2.4) reduces to

$$\iint_S \left(U\frac{\partial G}{\partial n} - G\frac{\partial U}{\partial n}\right) dS \;=\; 0. \tag{2.6}$$

Auxiliary function G was chosen $exp(jks)/s$, where s denotes the distance from P to the arbitrary point (x, y, z). It may be made it easy to think auxiliary function G as a "probe" which is used to investigate optical disturbance at point P. This auxiliary function at point P forms a virtual point source. It has singularity for $s = 0$ and there cannot be sources inside S since it is assumed that both U and G satisfy source-free Helmholtz wave equation in volume V, hence P must be excluded from the domain of integration. Therefore, it is convenient to surround P with a small sphere of radius ϵ and extend the integration throughout the volume between S and the surface S_ϵ of this sphere (See Figure 2.2). Finally one form of Kirchhoff's integral theorem is given by (See full derivation for Appendix A.1) (Ghatak, 2010)

$$U(P) = \frac{1}{4\pi}\iint_S \left[\frac{\partial U}{\partial n}\left(\frac{exp(jks)}{s}\right) - U\frac{\partial}{\partial n}\left(\frac{exp(jks)}{s}\right)\right] dS. \tag{2.7}$$

This is also known as Kirchhoff-Helmholtz integral formula.

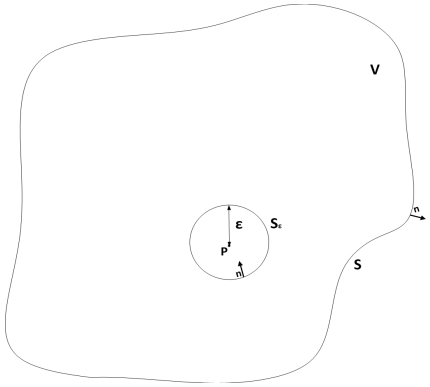

Figure 2.2. The domain of integration

Equation (2.7) states that as long as the point P is inside volume V, the light disturbance at the point P can be obtained only taking both U and $\partial U/\partial n$ at the boundaries of V, simply on S. This resultant makes us considered about boundary values for both U and $\partial U/\partial n$ on S.

Let's assume that the diffraction through an aperture in a planar screen is formulated by applying Kirchhoff's integral theorem. The closed surface for diffraction problem is made up of the aperture plane and a large partial sphere centered at the point of observation P, as shown in Figure 2.3. Accordingly the integral Equation (2.7) for the boundaries $\mathbb{A}$, $\mathbb{B}$, and $\mathbb{C}$ can be written as

$$U(P) = \frac{1}{4\pi}\left[\iint_{\mathbb{A}} + \iint_{\mathbb{B}} + \iint_{\mathbb{C}}\right]\left\{\frac{\partial U}{\partial n}\left(\frac{exp(jks)}{s}\right) - U\frac{\partial}{\partial n}\left(\frac{exp(jks)}{s}\right)\right\} dS. \tag{2.8}$$

Kirchhoff set the boundary values. Across the surface $\mathbb{A}$, the incident field and the diffracted field are the same, on the portion of $\mathbb{B}$ the field distribution and its normal derivative are zero (See Figure 2.3). These are called Kirchhoff's BC. However, this BC on $\mathbb{B}$ does not meet the theory of harmonic functions which are solutions of Laplace's equation ($\Delta U = 0$) in an arbitrary domain V. Since, if a harmonic function and its normal derivative is zero at any boundary on the surface, the function on the whole surface is vanished. As a matter of fact, the same situation is valid for the wave functions that satisfy source-free Helmholtz wave equation. This is not surprising, since when $k \to 0$ it becomes Laplace's equation and it also suggests that Green's functions for two equations differ only exponential term $exp(jks)$ and both have the same s^{-1} singularity.

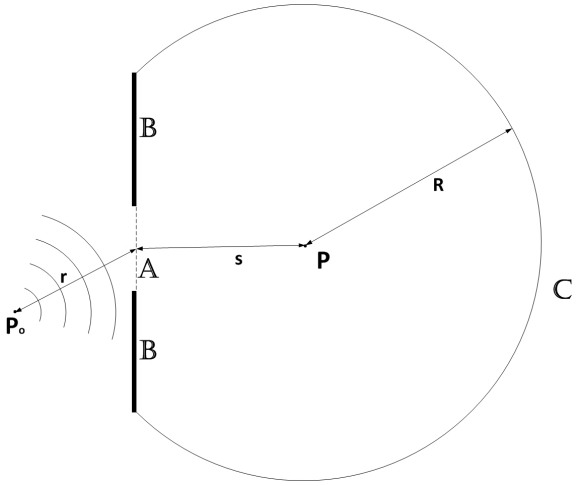

Figure 2.3. The integeration surfaces

The contradiction was solved by Sommerfeld. He chose two different auxiliary functions which also satisfy source-free Helmholtz wave equation due to the same reason. He introduced another virtual point source at $\tilde{P}$ which is a mirror image of P on the left side of the screen, alongside Kirchhoff's choice of auxiliary function that forms virtual point source at P. He assumed for the first auxiliary functions, sources at $\tilde{P}$ and at P are oscillating with the phase difference $180\,^\circ$ while for the second auxiliary function these sources have no phase difference between them. Their wavelengths are equal. First assumption yields auxiliary function zero on the surfaces both $\mathbb{A}$ and $\mathbb{B}$. It seems reasonable to make the real field U zero on the surface $\mathbb{B}$ (Dirichlet BC). The second assumption makes normal derivative of the auxiliary function to be zero on the surfaces both $\mathbb{A}$ and $\mathbb{B}$. In that case, normal derivative of the real field ($\partial U/\partial n$) assumed to be zero (Neumann BC). Both of the auxiliary functions prevent contribution from surface $\mathbb{B}$ and they comply with the property of the potential theory. In spite of the fact that the auxiliary functions

and the BC's are strictly different for three theorems, the resultant equations are nearly identical. Therefore, we follow Kirchhoff's theory as it has pointed out earlier section.

There is only contribution from portion $\mathbb{C}$ remains undetermined. If the radius R is chosen to be large, the integral over $\mathbb{C}$ will vanish. However, it is assumed that U is a monochromatic light wave ($\Delta\nu/\nu = 0$) which implies it is found all times and in all space by definition. One can avoid this argument by considering physically impossible to produce monochromatic light or more precisely introducing Sommerfeld radiation condition (See Appendix A.2). It is important theoretical result since only the outgoing waves are appropriate solution. Hence, the Equation (2.8) becomes

$$U(P) = \frac{1}{4\pi}\left[\iint_{\mathbb{A}} \frac{\partial U}{\partial n}\left(\frac{exp(jks)}{s}\right) - U\frac{\partial}{\partial n}\left(\frac{exp(jks)}{s}\right)\right] dS, \tag{2.9}$$

where $U = U_i = A\frac{exp(jkr)}{r}$, since it is assumed that on the surface $\mathbb{A}$ the field distribution U is the same as it would be when there is no obstruction. In addition to that, it is convenient to neglect $1/r$ and $1/s$ terms compared to k value, it is expressed

$$U(P) = \frac{jA}{2\lambda}\iint_{\mathbb{A}} \frac{exp(jk(r+s))}{rs}\left[cos(n,r) - cos(n,s)\right] dS, \tag{2.10}$$

where the angles are defined as in Figure 2.4. This is known as the Fresnel-Kirchhoff diffraction formula. Equation (2.7) is the one form of the formula, when it is multiplied by -1 or choosing partial derivative $\partial/\partial n$ in the inward normal direction at each point on S the other form is obtained. Since the intensity of the scalar wave function is $I = |U|^2$, these two forms have same the intensity value which is the primary interest.

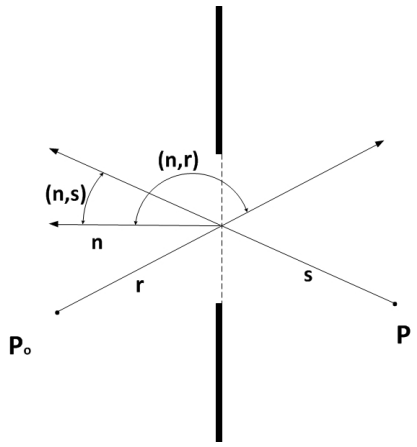

Figure 2.4. Illustration of angles to derive Fresnel-Kirchhoff diffraction formula

New boundaries might be chosen to obtain an integral theorem for the propagation of wavefront. The result also gives the explicit formula for the inclination factor that is remained undefined in Huygens-Fresnel principle. Let us assume that portion W of an incident wavefront filled the aperture (See Figure 2.5). On W, $\hat{r_0}$ and $\hat{n}$ are reverse directed, so $cos(n, r_0) = -1$. Also, the angle of diffraction is set $\chi = (r_0, s)$ due to the assumption that we make, Equation (2.10) is written as

$$U(P) \;=\; -\frac{j}{2\lambda}\frac{A\,exp(jkr_0)}{r_0}\iint_W \frac{exp(jks)}{s}\,(1+cos\chi)\,dS. \tag{2.11}$$

Contribution from the element dW of the wavefront

$$-\frac{j}{2\lambda}\frac{A\,exp(jkr_0)}{r_0}\,\frac{exp(jks)}{s}\,(1+cos\chi)\,dS, \tag{2.12}$$

which can be compared with the Equation (2.1). It gives the explicit formula for inclination factor

$$K(\chi) \;=\; -\frac{j}{2\lambda}(1+cos\chi). \tag{2.13}$$

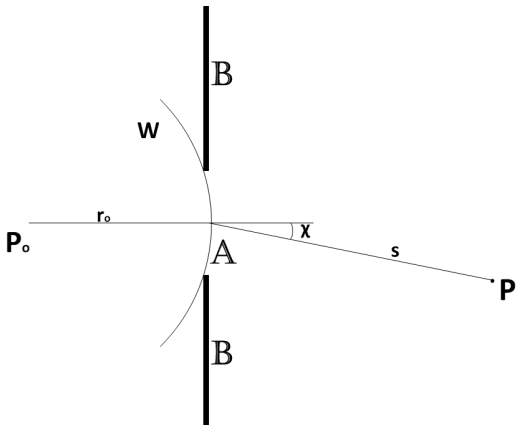

Figure 2.5. Illustrating new boundaries

Consequently, Huygens-Fresnel equation with the recovered inclination factor as in Equation (2.11), might be taken into account once the field distribution of spherical wavefront at an arbitrary point is wanted to be determined. Basically, it is regarded as wavefront tracing. Moreover, some approximations can be made to make Equation (2.11) suitable for different kind of problems such as diffraction from the phase objects.

CHAPTER 3

MATHEMATICAL MODEL FOR PHASE DIFFRACTION

In this chapter, the consequences of Kirchhoff's scalar diffraction theory is implemented when it is applied to the phase objects, specially fiber optic and coated fiber optic. This chapter is to construct theoretical basis for the thesis.

3.1. Diffraction From Phase Objects

Diffraction effects of various kind of apertures on wavefronts can be found easily with the help of diffraction formula as it has pointed out in former section. These kind of problems can be found in details in many optical textbooks unlike diffraction effects from phase object. The diffraction by a smooth transparent phase object of any shape was investigated geometrically by Yung Ming Chen (Chen, 1964).

Fresnel diffraction effect from phase object, in particular, from fixed and variable phase steps are very rich subject and yields several application since phase of the wave is more sensitive to the variation in refractive index, thickness or both than is the amplitude. This feature what we exploit makes it powerful candidate for optical sensors. These effects were studied by several authors (Raman and Ramakrishna Rao (1926), Faust (1950), Sussman (1962)) and more comprehensive studies have been done very recently by Tavassoly et al. (2012).

Diffraction effects become noticeable when wavefront bears sharp change in phase as it has mentioned in the beginning of section. Sharp change in the phase can be easily implemented by sending light beam through a phase step or transmitting light beam through a phase object with an abrupt change in refractive index or thickness (Tavassoly et al., 2005). It is called phase diffraction.

3.1.1. Theoretical Approach

Theory of diffraction from phase object is based on Huygens-Fresnel principle or strictly speaking Fresnel-Kirchhoff diffraction integral, since the diffraction from phase object is nothing but tracing of the wavefronts. We trace wavefronts after it transmitted through optical fiber.

3.1.1.1. Diffraction from Fiber Optic

Diffraction from cylindrical transparent object and its intensity distribution at an arbitrary point are the main part of the thesis. Diffraction effects of a plane wave from a cylindrical rod such as step index optical fiber whose radii are a and b, respectively, are examined (Sabatyan and Tavassoly, 2007). Hence, the usage of Fresnel-Kirchhoff integral is appropriate to find disturbance on the transmission screen (See Figure 3.1).

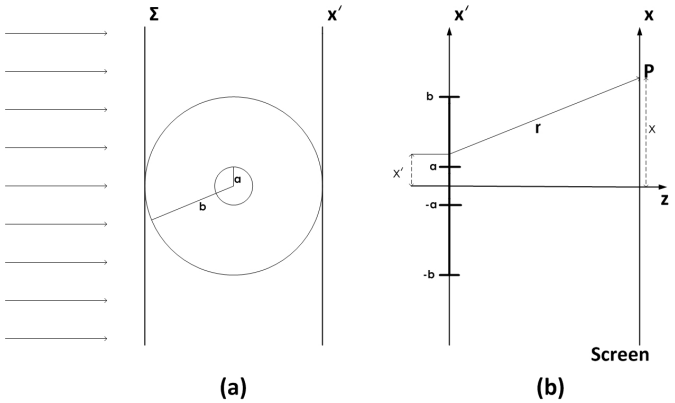

Figure 3.1. (a) Plane wave transmission from optical fiber, (b) Diffraction geometry for optical fiber

Small angle approximation which makes $cos\chi$ zero due to plane wave, is applied and inclination factor evolves another form for the cylindrical wavefronts. Fresnel-Kirchhoff diffraction integral equation for the cylindrical diffracted wave is written as (Amiri and M.Tavassoly, 2006)

$$U(P) \;=\; \sqrt{-\frac{j}{\lambda}}A \int exp(jkr_0)\frac{exp(jkr)}{\sqrt{r}}\,dx'. \tag{3.1}$$

From the theoretical point of view, it is an indeed aperture problem that we investigated earlier sections. In our case there is no portion $\mathbb{B}$ and Sommerfeld radiation condition is indeed preserved. The only contribution is from surface $\mathbb{A}$ that lies in between $-\infty$ to $+\infty$ because we send a plane wave, that means we are in Fresnel region not in reactive region. Hence, it can not be applied any kind of far field approximation but paraboloidal wave approximation (Saleh and Teich, 2007). The very well known solution of Helmholtz equation in spherical coordinates yields the spherical wave $u(r) = exp(jkr)/r$, where r is represented in cartesian coordinates as $r = \sqrt{x^2 + y^2 + z^2}$. Using the approximation based on Taylor series expansion:

$$\begin{aligned} r &= z\sqrt{1+\theta^2} \\ &= z\left(1 + \frac{\theta^2}{2} - \frac{\theta^4}{8} + ...\right) \\ &\approx z\left(1 + \frac{\theta^2}{2}\right) \\ &= z + \frac{x^2+y^2}{2z}, \end{aligned} \tag{3.2}$$

where $\theta = \frac{x+y}{z}$. The Equation (3.2) is substituted for the solution of Helmholtz equation in spherical coordinates, moreover substituting a less accurate expression $r \approx z$ into the magnitude, $u(r)$ becomes

$$u(r) \;=\; \frac{1}{z}\, exp(jkz)\, exp\left[jk\left(\frac{x^2+y^2}{2z}\right)\right], \tag{3.3}$$

which is so-called Fresnel approximation of the spherical wave. It plays important role in diffraction. Equation (3.3) is substituted into Equation (3.1), the diffraction integral for the cylindrical diffracted wave can be expressed as (Sabatyan and Tavassoly, 2007)

$$U(P) \;=\; K \int exp(jkr_0) exp\left[jk\left(\frac{(x-x')^2}{2z}\right)\right]\, dx', \tag{3.4}$$

where $K = \sqrt{-\frac{j}{\lambda}} A\, \frac{exp(jkz)}{\sqrt{z}}$. Equation (3.4) is essential equation for cylindrical diffracted wave problems. It might be modified in the sense of layer boundaries.

In order to obtain the amplitude of the diffracted wave on the screen at an arbitrary point for the two layer geometry (simple fiber optic), it is convenient to define new parameters with respect to the Figure 3.2(a), where

$$\begin{aligned} &|GC| = x' \ , && |GD| = a \ , && |GE| = b \ , \\ &|CD| = \sqrt{a^2 - x'^2} \ , && |CE| = \sqrt{b^2 - x'^2} \ , && |EB| = b - \sqrt{b^2 - x'^2}. \end{aligned} \tag{3.5}$$

Similarly for the Figure 3.2(b), where

$$\begin{aligned} &|GF| = x' \ , && |GR| = b \ , \\ &|FR| = \sqrt{b^2 - x'^2} \ , && |RQ| = b - \sqrt{b^2 - x'^2}. \end{aligned} \tag{3.6}$$

Since integration is done with respect to x', they are in common both of the Equation (3.5) and Equation (3.6).

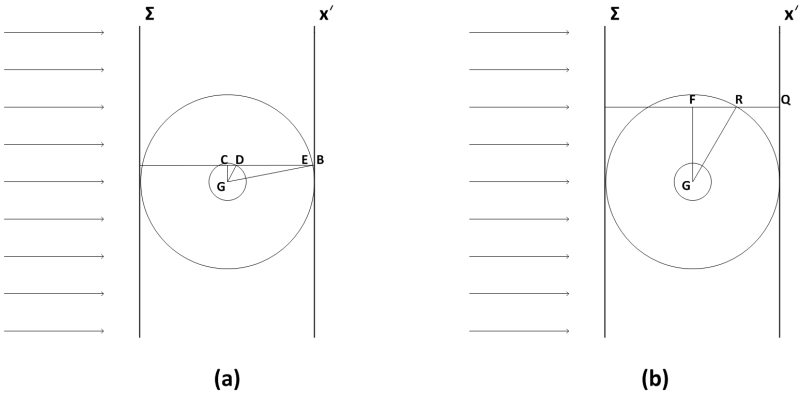

Figure 3.2. Optical fiber geometry

Particular region of wavefront proceeds different optical paths. Therefore, optical phases between planes Σ and x', can be defined as follows (Sabatyan and Tavassoly, 2009)

$$\phi_{su} = 2kcn_s, \qquad |x'| > b \tag{3.7}$$

$$\phi_1 = \; 2k[(b - \sqrt{b^2 - x'^2})n_s + (\sqrt{b^2 - x'^2})n_{cl}], \qquad a < |x'| < b \tag{3.8}$$

$$\phi_2 = 2k[(b - \sqrt{b^2 - x'^2})n_s + (\sqrt{b^2 - x'^2} - \sqrt{a^2 - x'^2})n_{cl} + (\sqrt{a^2 - x'^2})n_{co}], \quad |x'| < a \tag{3.9}$$

where n_s, n_{cl}, n_{co}, and k are the refractive indices of the surrounding medium, the cladding, the core, and the wave number, respectively. Denoting

$$\phi_{cl} \;=\; 2k(n_{cl} - n_s)\sqrt{b^2 - x'^2}, \tag{3.10}$$

$$\phi_{co} \;=\; 2k(n_{co} - n_{cl})\sqrt{a^2 - x'^2}. \tag{3.11}$$

The diffraction integral for $x' < -b$ becomes,

$$U_1(P) \;=\; K \int_{-\infty}^{-b} exp(-j\phi_{su}) exp\left[j\frac{2\pi}{\lambda}\left(\frac{(x - x')^2}{2z}\right)\right] dx'. \tag{3.12}$$

Similarly for the intervals $-b < x' < -a$, $-a < x' < a$, $a < x' < b$, and $x' > b$, the diffraction integrals take the form of, respectively;

$$U_2(P) \;=\; K \int_{-b}^{-a} exp(-j[\phi_{su} + \phi_{cl}]) exp\left[j\frac{2\pi}{\lambda}\left(\frac{(x - x')^2}{2z}\right)\right] dx', \tag{3.13}$$

$$U_3(P) = K\int_{-a}^{a} exp(-j[\phi_{su}+\phi_{cl}+\phi_{co}])exp\left[j\frac{2\pi}{\lambda}\left(\frac{(x-x')^2}{2z}\right)\right]dx', \quad (3.14)$$

$$U_4(P) = K\int_{a}^{b} exp(-j[\phi_{su}+\phi_{cl}])exp\left[j\frac{2\pi}{\lambda}\left(\frac{(x-x')^2}{2z}\right)\right]dx', \quad (3.15)$$

$$U_5(P) = K\int_{b}^{\infty} exp(-j\phi_{su})exp\left[j\frac{2\pi}{\lambda}\left(\frac{(x-x')^2}{2z}\right)\right]dx'. \quad (3.16)$$

The total field at point P are given by

$$U(P) = U_1(P) + U_2(P) + U_3(P) + U_4(P) + U_5(P), \quad (3.17)$$

and it becomes in expanded form

$$\begin{aligned} U(P) = A\sqrt{\frac{-j}{2}}\exp(jkz)\exp(-j2kbn_s)\Big\{1 + C(\alpha) - C(\beta) + j\big[1 + S(\alpha) - S(\beta)\big] \\ + \sqrt{\frac{2}{\lambda z}}\Big(\int_{-b}^{-a} exp(-j2k\sqrt{b^2-x'^2}(n_{cl}-n_s))exp\left[jk\frac{(x-x')^2}{2z}\right]dx' \\ + \int_{-a}^{a} exp(-j2k(\sqrt{b^2-x'^2}\{n_{cl}-n_s\} + \sqrt{a^2-x'^2}\{n_{co}-n_{cl}\}))exp\left[jk\frac{(x-x')^2}{2z}\right]dx' \\ + \int_{a}^{b} exp(-j2k\sqrt{b^2-x'^2}(n_{cl}-n_s))exp\left[jk\frac{(x-x')^2}{2z}\right]dx'\Big)\Big\}, \end{aligned} \quad (3.18)$$

where C and S are Fresnel cosine and sine functions that are explained in section 3.1.4. Their dependency on α and β indicate $\sqrt{\frac{2}{\lambda z}}(x-b)$ and $\sqrt{\frac{2}{\lambda z}}(x+b)$ respectively. To obtain normalized results, the Equation (3.19) is divided by field when there is no fiber

$$U_{nf}(P) = A\exp(jkz)\exp(-j2kbn_s). \quad (3.19)$$

Intensity is the main concern here and it is formed for the two layer geometry with a surrounded medium

$$I = \frac{U(P)U^*(P)}{U_{nf}(P)U^*_{nf}(P)}. \quad (3.20)$$

where * represents the complex conjugate.

3.1.1.2. Diffraction From Three Layer Phase Object

Three layer geometry simply refers fiber optic with coated dielectric radius c and refractive index n_p (See Figure 3.3). We follow the same procedure as we have done in previous chapter to obtain the mathematical model for the coated fiber optic. The whole procedure is to find optical disturbance at an arbitrary point on the screen after wavefront is transmitted through coated optical fiber.

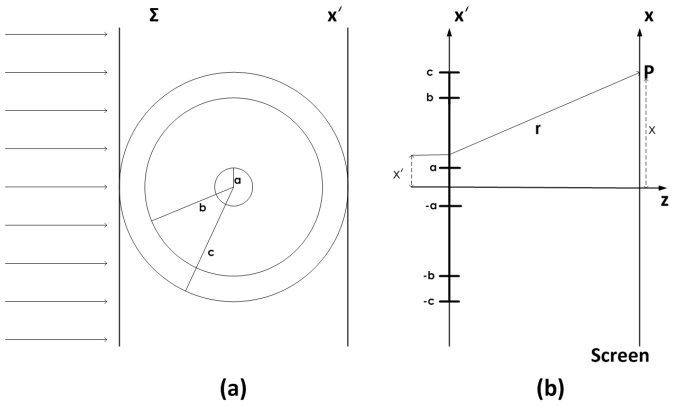

Figure 3.3. (a) Plane wave transmission from coated optical fiber, (b) Diffraction geometry for coated optical fiber

Optical path lengths are defined by following the same procedure in the last section, simply trying to obtain wavefront after it transmits three layer geometry

$$\phi_{su} = 2kcn_s, \qquad |x'| > c \tag{3.21}$$

$$\phi_1 = 2k[(c - \sqrt{c^2 - x'^2})n_s + (\sqrt{c^2 - x'^2})n_p], \qquad b < |x'| < c \tag{3.22}$$

$$\phi_2 = 2k[(c - \sqrt{c^2 - x'^2})n_s + (\sqrt{c^2 - x'^2} - \sqrt{b^2 - x'^2})n_p + (\sqrt{b^2 - x'^2})n_{cl}], \quad b < |x'| < a \tag{3.23}$$

$$\phi_3 = 2k[(c - \sqrt{c^2 - x'^2})n_s + (\sqrt{c^2 - x'^2} - \sqrt{b^2 - x'^2})n_p + (\sqrt{b^2 - x'^2} - \sqrt{a^2 - x'^2})n_{cl} + (\sqrt{a^2 - x'^2})n_{co}], \quad |x'| < a. \tag{3.24}$$

Denoting

$$\phi_p = 2k(n_p - n_s)\sqrt{c^2 - x'^2} \tag{3.25}$$

$$\phi_{cl} = 2k(n_{cl} - n_p)\sqrt{b^2 - x'^2}, \tag{3.26}$$

$$\phi_{co} = 2k(n_{co} - n_{cl})\sqrt{a^2 - x'^2} \tag{3.27}$$

The diffraction integral for $x' < -c$ becomes,

$$U_1(P) = K \int_{-\infty}^{-c} exp(-j\phi_{su}) exp\left[j\frac{2\pi}{\lambda}\left(\frac{(x-x')^2}{2z}\right)\right] dx'. \quad (3.28)$$

Similarly for the intervals $-c < x' < -b$, $-b < x' < -a$, $-a < x' < a$, $a < x' < b$, $b < x' < c$, and $x' > c$, the diffraction integrals become, respectively;

$$U_2(P) = K \int_{-c}^{-b} exp(-j[\phi_{su} + \phi_p]) exp\left[j\frac{2\pi}{\lambda}\left(\frac{(x-x')^2}{2z}\right)\right] dx', \quad (3.29)$$

$$U_3(P) = K \int_{-b}^{-a} exp(-j[\phi_{su} + \phi_p + \phi_{cl}]) exp\left[j\frac{2\pi}{\lambda}\left(\frac{(x-x')^2}{2z}\right)\right] dx', \quad (3.30)$$

$$U_4(P) = K \int_{-a}^{a} exp(-j[\phi_{su} + \phi_p + \phi_{cl} + \phi_{co}]) exp\left[j\frac{2\pi}{\lambda}\left(\frac{(x-x')^2}{2z}\right)\right] dx', \quad (3.31)$$

$$U_5(P) = K \int_{a}^{b} exp(-j[\phi_{su} + \phi_p + \phi_{cl}]) exp\left[j\frac{2\pi}{\lambda}\left(\frac{(x-x')^2}{2z}\right)\right] dx', \quad (3.32)$$

$$U_6(P) = K \int_{b}^{c} exp(-j[\phi_{su} + \phi_p]) exp\left[j\frac{2\pi}{\lambda}\left(\frac{(x-x')^2}{2z}\right)\right] dx', \quad (3.33)$$

$$U_7(P) = K \int_{c}^{\infty} exp(-j\phi_{su}) exp\left[j\frac{2\pi}{\lambda}\left(\frac{(x-x')^2}{2z}\right)\right] dx'. \quad (3.34)$$

The total field at point P are given by

$$U(P) = U_1(P) + U_2(P) + U_3(P) + U_4(P) + U_5(P) + U_6(P) + U_7(P), \quad (3.35)$$

the total field at point P can be obtained by considering Equation (3.4) in the expanded form;

$$U(P) = A\sqrt{\frac{-j}{2}}\exp(jkz)\exp(-j2kbn_s)\Big\{1 + C(\gamma) - C(\xi) + j\big[1 + S(\gamma) - S(\xi)\big] + \sqrt{\frac{2}{\lambda z}}\Big(\int_{-c}^{-b} exp(-j2k\sqrt{c^2 - x'^2}(n_p - n_s))exp\Big[jk\frac{(x-x')^2}{2z}\Big]\,dx' + \int_{-b}^{-a} exp(-j2k(\sqrt{c^2 - x'^2}(n_p - n_s) + \sqrt{b^2 - x'^2}(n_{cl} - n_p)))exp\Big[jk\frac{(x-x')^2}{2z}\Big]\,dx' + \int_{-a}^{a} exp(-j2k(\sqrt{c^2 - x'^2}(n_p - n_s) + \sqrt{b^2 - x'^2}(n_{cl} - n_p) + \sqrt{a^2 - x'^2}(n_{co} - n_{cl})) \times exp\Big[jk\frac{(x-x')^2}{2z}\Big]\,dx' + \int_{a}^{b} exp(-j2k(\sqrt{c^2 - x'^2}(n_p - n_s) + \sqrt{b^2 - x'^2}(n_{cl} - n_p))) \times exp\Big[jk\frac{(x-x')^2}{2z}\Big]dx' + \int_{b}^{c} exp(-j2k\sqrt{c^2 - x'^2}(n_p - n_s))exp\Big[jk\frac{(x-x')^2}{2z}\Big]dx'\Big)\Big\}. \tag{3.36}$$

Fresnel cosine and sine functions' dependency on γ and ξ indicate $\sqrt{\frac{2}{\lambda z}}(x - c)$ and $\sqrt{\frac{2}{\lambda z}}(x + c)$, respectively. To obtain the normalized results, Equation (3.36) is divided by amplitude of the incident field when there is no coated fiber Equation (3.19). Intensity becomes for three layer geometry with a surrounded medium

$$I = \frac{U(P)U^*(P)}{U_{nf}(P)U^*_{nf}(P)}. \tag{3.37}$$

3.1.2. Numerical Calculations of Equations

In this section, we show how to solve equation arrays (3.12)-(3.16) and (3.28)-(3.34). Numerical integration method and Fresnel integrals that may be solved under favour of Cornu's spiral are presented.

3.1.2.1. Quadrature Method

Since not all integrals can be solved analytically, the numerical integration methods have been developed. Numerical integration methods are generally based on finding polynomial $P(x)$ that interpolates the function $f(x)$. Instead of integrating the function,

polynomial might be used as an approximation to the function.

$$\int_a^b f(x)dx \approx \int_a^b P(x)dx = \int_a^b \Big(\sum_{i=1}^{n} f(x_i)L_i(x) \Big) dx = \sum_{i=1}^{n} w_i f(x_i), \tag{3.38}$$

where

$$w_i = \int_a^b L_i(x)dx. \tag{3.39}$$

The values w_i and x_i are called weights and nodes respectively. The polynomials $L_i(x)$ are the Lagrange interpolating polynomials

$$L_i(x) = \prod_{k=1, k\neq i}^{n} \frac{x - x_k}{x_i - x_k}. \tag{3.40}$$

This is called Newton-Cotes quadrature formula. It gives basic mathematical insight for well known trapezoidal rule, Simpson's rules, and Boole's rule. This quadrature formula based on equally spaced abscissas.

Degree of exactness of the quadrature rule which is the important characteristic of every quadrature formula is m if this quadrature rule yields exact results for all the polynomial of degree $d \leq m$. Degree of exactness of the Newton-Cotes quadrature formula is $m + 1$.

Gauss quadrature is another type of quadrature rule. It is closely related to Newton-Cotes quadrature formula in the sense of utilizing Lagrange interpolating polynomials. The key idea stands behind Gauss quadrature is a clever choice of abscissas in order to maximize the degree of exactness. Orthogonal polynomials and their zeros on the line play important role to maximize degree of exactness. Gaussian quadrature rule is exact for the polynomials of degree $d \leq 2m - 1$, if m nodes are chosen the zeros of the polynomials. The zeros of the corresponding orthogonal polynomial and weights of Gauss quadrature can be computed by using Golub-Welsch algorithm (Golub and Welsch, 1969). The starting point of constructing the algorithm is three-term recurrence relation property of orthogonal polynomials. Writing these relations in a matrix form yields eigenvalue equation. Eigenvalues of the matrix is the nodes of the corresponding Gauss quadrature, in other words zeros of the corresponding polynomial.

Gauss-Kronrod quadrature is a different kind of Gauss quadrature. There are extra m Kronrod nodes which indicate corresponding zeros of Stieltjes polynomial (Laurie, 1997). The difference between Gauss and Kronrod quadrature approximations yields error of the integration.

When Equation arrays (3.13)-(3.15) and (3.29) - (3.33) are considered, it is needed to evaluate numerically. Since integrand might be considered conventional oscillatory function in small interval a to b, it is convenient to use adaptive Gauss-Kronrod Quadrature. Otherwise, highly oscillation integration methods should be used. In MATLAB, there is a function $quadgk$ which uses $G7 - K15$ points adaptive quadrature to evaluate integrals.

3.1.2.2. Fresnel Integrals

Equations (3.12), (3.16), (3.28), and (3.34) whose boundaries extend infinity remains undetermined. There are some techniques to evaluate these kind of integrals, but we choose graphical device to evaluate. Only the Equation (3.12) is taken into account for simplicity, the others can be evaluated following the same steps. It can be written as

$$U_1(Q) = K' \int_{-\infty}^{-b} exp\left[j\frac{2\pi}{\lambda}\left(\frac{(x-x')^2}{2z}\right)\right] dx', \tag{3.41}$$

where $K' = Kexp(-j\phi_{su})$. Let us define a new parameter

$$\tau = \sqrt{\frac{2}{\lambda z}}(x - x'), \tag{3.42}$$

and dx' becomes

$$dx' = -\sqrt{\frac{\lambda z}{2}}d\tau. \tag{3.43}$$

Considering both the former equation and famous Euler's formula, Equation (3.41) takes the form of

$$U_1(Q) = K''\left[\int_{+\infty}^{\zeta} cos\left(\frac{\pi}{2}\tau^2\right)d\tau + j\int_{+\infty}^{\zeta} sin\left(\frac{\pi}{2}\tau^2\right)d\tau\right], \tag{3.44}$$

where $K'' = -K'\sqrt{\frac{\lambda z}{2}}$ and $\zeta = \sqrt{\frac{2}{\lambda z}}(x + b)$. First integration of the Equation (3.44) is called Fresnel cosine integral, whereas second integration is called Fresnel sine integral. These integrals play a significant role solving diffraction problems, in particular near field regions. Cornu's Spiral is used in order to evaluate the Fresnel integrals (See Figure 3.4). It is a graphical device whose horizontal axes $C(\tau)$ and vertical axes $S(\tau)$ represent

$$C(\tau) = \int_0^{\tau} cos\left(\frac{\pi}{2}\tau^2\right)d\tau, \tag{3.45}$$

$$S(\tau) = \int_0^{\tau} sin\left(\frac{\pi}{2}\tau^2\right)d\tau. \tag{3.46}$$

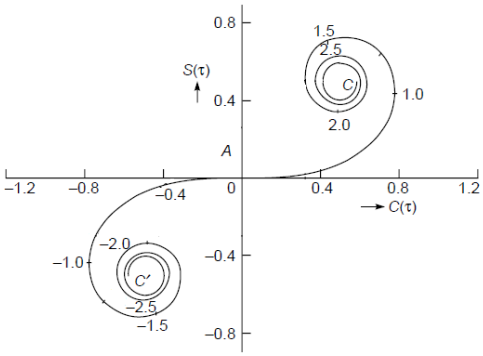

Figure 3.4. Cornu's Spiral

Similar treatment is applied to the Equation (3.16) and overall effects of the infinity bounded integrals which arise due to the plane wave, are calculated easily. In MATLAB, there are functions $fresnelc$ and $fresnels$ to evaluate Fresnel cosine and sine integrals, respectively.

CHAPTER 4

REFRACTIVE INDEX SENSING

In this chapter, it is shown how to sense surrounding medium's refractive index by using phase diffraction method to make sure the method is valid. We exploited this method for detecting of adulteration in virgin olive oil.

4.1. Refractive Index Origins

In the simplest approach of an atom, electrons are considered to be bounded elastically to the nucleus. The variation of electron's position is governed by the equation of motion for an oscillator. This classical approach was proposed by Lorentz in the later nineteenth century. More precise treatment requires quantum mechanical approach.

Refractive index originally arises when electric field is applied to the medium. Applied electric field gives rise to dipole moment atomically or polarization volumetrically. Polarization and electric field compound electric displacement vector together. Electric displacement vector is proportional to relative permittivity which is a square of refractive index. It might have imaginary part for the lossy or gainful mediums, it is not taken into account in this thesis.

Refractive index is one of the most crucial parameter of the material. Precise determination of refractive index gives more insight about the optical properties of material. There are some techniques to identify refractive index of the liquids. Interferometric methods (Angelis et al. (2000), Musso et al. (2000)), diffraction grating based methods (Durán-Ramìrez et al. (2014), Lu et al. (2007)), long period fiber grating (LPG) based methods (James and Tatam (2003), Huang et al. (2013), Tsuda and Urabe (2009)), and phase diffraction method which is used in this thesis (Sabatyan and Tavassoly, 2009) are some of them. Additionally, Abbe refractometers are standard tool for measuring refractive index of the liquids.

4.2. Surrounding Liquid Medium Refractive Index Sensing

We used phase diffraction method to obtain refractive index of the surrounding medium. Interesting feature of the method is the sensitivity of index of refraction of the liquid that surrounds cladding of the fiber. Phase diffraction from fiber optic with a surrounding medium is explained in the former section comprehensively. The surrounding medium's refractive index (n_s) can be obtained precisely, provided that fiber's properties and the distance between fiber and detector are very well known as in the Equation (3.18).

4.2.1. Olive Oil Adulteration Detection

Adulteration of oils is currently big concern in the food industry due to high price of virgin olive oil. Nowadays there are some methods to detect adulteration in olive oils such as long period fiber grating based (Libish et al., 2013), Abbe refractometer based (Ariponnammal, 2012), and infrared (IR) spectroscopy with chemometric (Sun et al. (2015), Gurdeniz and Ozen (2009)). As it is indicated both (Libish et al., 2013) and (Ariponnammal, 2012) refractive index variation of the olive oil is ended up with detection of adulteration.

We used phase diffraction method to detect adulteration of olive oils in terms refractive index. Because, the method is quite sensitive external medium refractive index changes and it is easy to implement.

4.2.2. Experimental Procedure

A schematic of the experimental setup is sketched in Figure 4.1. Experimental procedure begins with conversion output of the He-Ne laser of wavelength 632.8 nm light beam to plane wave. Classical beam expander is used for this purpose. It converts Gaussian beam to plane wave. The acquired plane wave sent is through the sample perpendicular to its axis. Piece of step index fiber is immersed into the rectangle silica cell. This cell is filled with a sample whose refractive index value is to be determined and placed perpendicular to the plane wave. The intensity distributions are recorded by a charge coupled device (CCD) camera of pixel size 17 μm (H) $\times$ 11 μm (V) before and after immersing fiber. Dividing latter intensity distribution by the former one gives the normalized intensity distribution.

Fiber optics specifications are needed exactly. Fiber cladding and core radii are b = 62.5 μm, and a = 2.2 μm , respectively and refractive indices of the cladding and core are n_{cl} = 1.4537, and n_{co} = 1.4591 respectively, according to data sheet of 780-HP Nufern Single Mode Fiber (Nufern, 2013). The distance in between fiber and CCD camera is varies between 3.5 cm and 4.2 cm.

Olive oil is selected for the present study to detect adulteration and it mixed with sunflower oil in different percentages. In order to detect adulteration, normalized intensity distribution on the Fresnel diffraction patterns are fitted the mathematical model by using least-squares method.

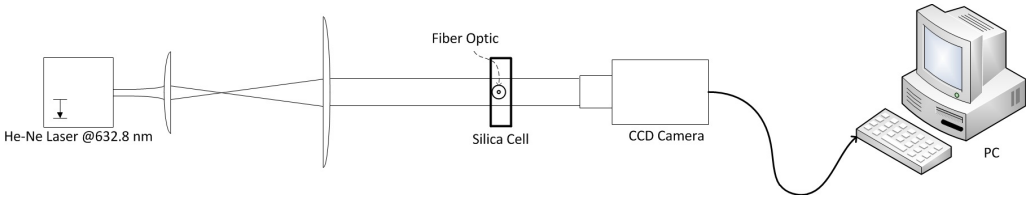

Figure 4.1. Top view of experimental setup for determining refractive index of the surrounding medium

4.2.3. Results

Three different olive oil mixed with sunflower oil in different percentages, pure olive oil, pure sunflower oil and pure water are selected to show the dependency on surrounding medium. These percentages are 10%, 30%, and 40% oil solutions. All solutions were prepared carefully. In order to analyze samples and compare results to the our proposed method, oil mixtures and pure ones were measured by RE50 digital refractometer (Mettler Toledo, 2003). Refractometer results were not in agreement with diffraction results (See Figure 4.8).

The refractive index of the pure water matches with the expected value as it is shown in Figure 4.2. Uncertainty is about $\pm\ 8\ \times\ 10^{-5}$ for the pure water (Kedenburg et al., 2012).

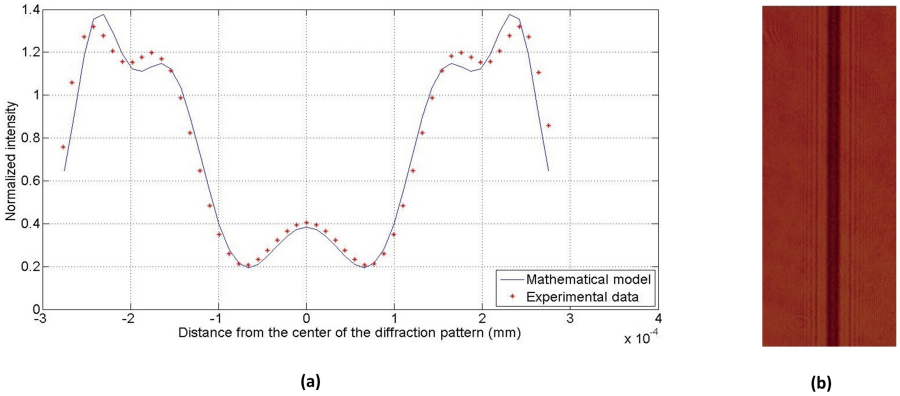

Figure 4.2. Surrounding refractive index determination (distance ≈ 4.1 cm) : (a) The dots are normalized experimental intensity distribution, the curve is the theoretical intensity fitted n_s = 1.33198 (b) Diffraction pattern recorded by CCD of a laser beam diffracted by optical fiber surrounded by pure water whose refractive index is 1.33198

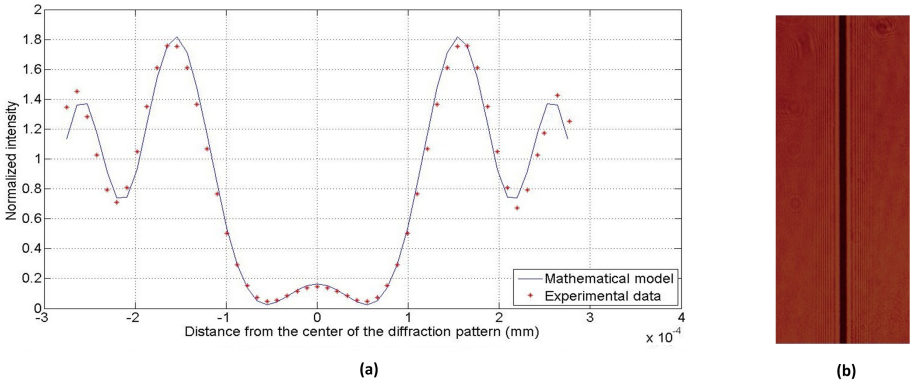

Figure 4.3. Surrounding refractive index determination (distance ≈ 4.1 cm) : (a) The dots are normalized experimental intensity distribution, the curve is the theoretical intensity fitted n_s = 1.46786 (b) Diffraction pattern recorded by CCD of a laser beam diffracted by optical fiber surrounded by pure olive oil whose refractive index is 1.46786

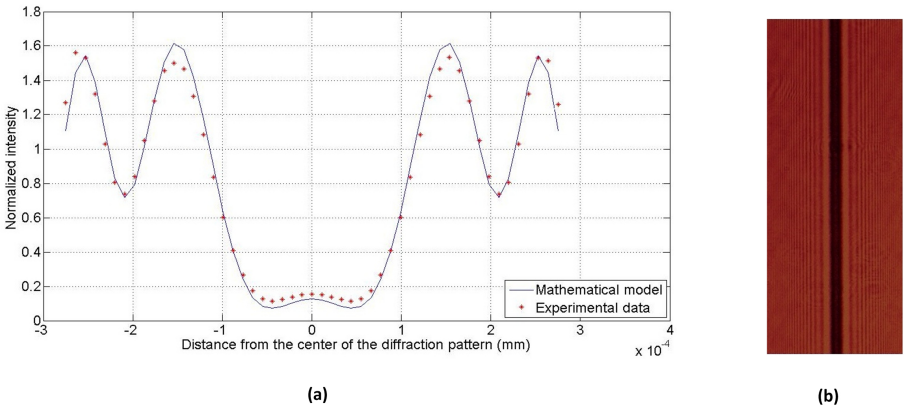

Figure 4.4. Surrounding refractive index determination (distance $\approx$ 4.2 cm) : (a) The dots are normalized experimental intensity distribution, the curve is the theoretical intensity fitted n_s = 1.46837 (b) Diffraction pattern recorded by CCD of a laser beam diffracted by optical fiber surrounded by 90% olive oil 10% sunflower oil mixture whose refractive index is 1.46837

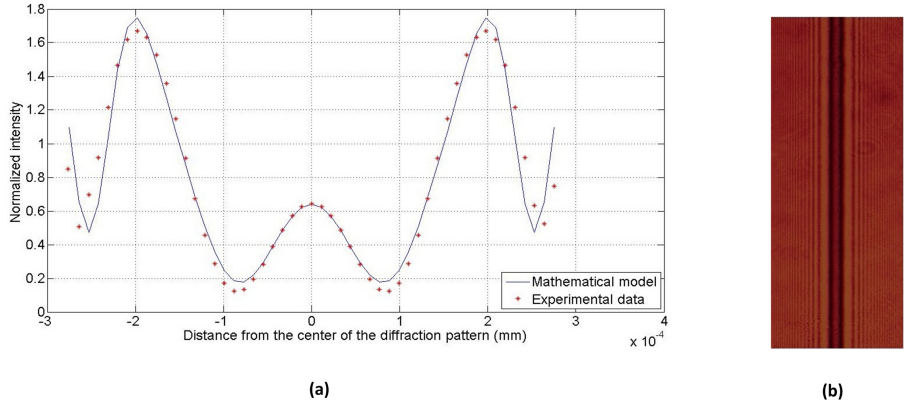

Figure 4.5. Surrounding refractive index determination (distance $\approx$ 3.6 cm) : (a) The dots are normalized experimental intensity distribution, the curve is the theoretical intensity fitted n_s = 1.47075 (b) Diffraction pattern recorded by CCD of a laser beam diffracted by optical fiber surrounded by 70% olive oil 30% sunflower oil mixture whose refractive index is 1.47075

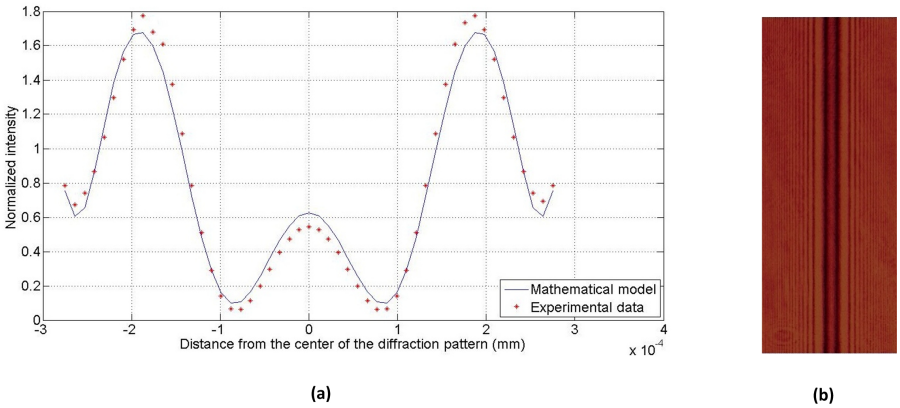

Figure 4.6. Surrounding refractive index determination (distance $\approx$ 4 cm) : (a) The dots are normalized experimental intensity distribution, the curve is the theoretical intensity fitted n_s = 1.47119 (b) Diffraction pattern recorded by CCD of a laser beam diffracted by optical fiber surrounded by 60% olive oil 40% sunflower oil mixture whose refractive index is 1.47119

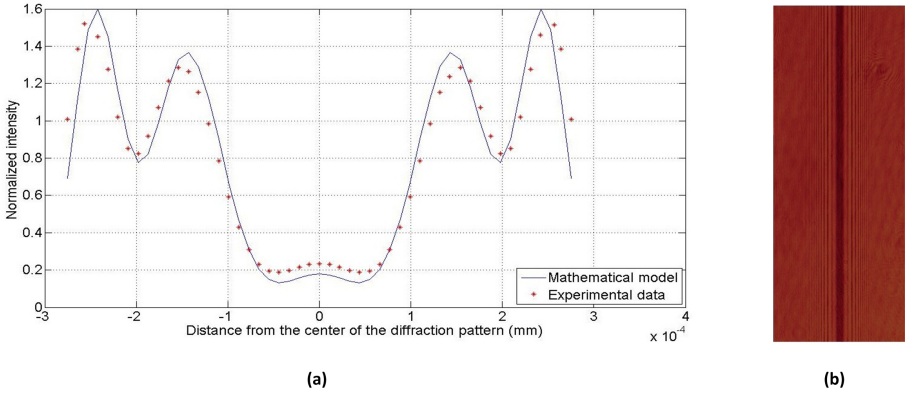

Figure 4.7. Surrounding refractive index determination (distance $\approx$ 4 cm) : (a) The dots are normalized experimental intensity distribution, the curve is the theoretical intensity fitted n_s = 1.47383 (b) Diffraction pattern recorded by CCD of a laser beam diffracted by optical fiber surrounded by pure sunflower oil whose refractive index is 1.47383

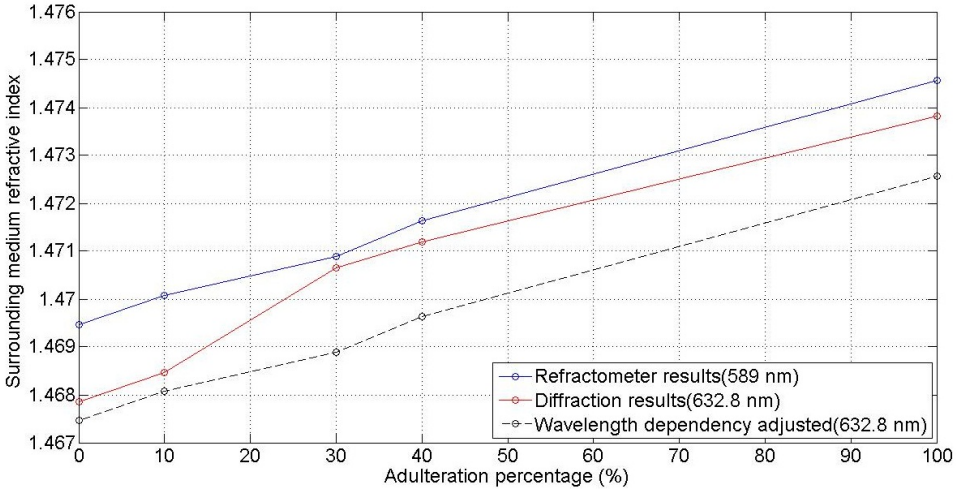

Figure 4.8. Comparison between the refractometer results, diffraction results, and wavelength dependency adjusted for the refractometer results

In Figure 4.8, 0% and 100% indicate pure olive oil and pure sunflower oil, respectively. The differences might be arisen due to wavelength dependency of refractive indices. Refractometer uses light whose wavelength 589 nm while we use that of 632.8 nm. As it is indicated in Yunus et al. (2009) refractive index of the olive oil differences for the 589 nm wavelength and 632.8 wavelength is approximately 2×10^{-3}. Hence these disparities can be attributed to the wavelength dependency of the refractive index (See Table 4.1).

Samples	Refractive Index (Diffraction)	Refractive Index (Refractometer)	Uncertainty
Pure Olive Oil	1.46786	1.46946	1.6×10^{-3}
10% solution	1.46847	1.47008	1.61×10^{-3}
30% solution	1.47066	1.47089	2.3×10^{-4}
40% solution	1.47119	1.47164	4.5×10^{-4}
Pure Sunflower Oil	1.47383	1.47456	7.3×10^{-4}

Table 4.1. Comparison of refractive index values between diffraction based measurements and refractometer based measurements

CHAPTER 5

OPTICAL DIELECTRIC FILMS ON CURVED SURFACES

In this chapter, it is shown how to determine thickness of the optical dielectric films, in particular, polyvinyl alcohol on curved surfaces such as optical fibers. Phase diffraction method is used for this objective and it yields good results.

Fiber optic coatings prevent fiber optic from mechanical and chemical damages conventionally (Wojcik et al., 2006). On the other hand, coated films are to support to modulate light signals when specific measurand is exposed. This idea allows to develop sensitivity enhanced fiber optic sensors in conjunction with thin films (Renoirt et al. (2013), Yang and Dai (2012)). For that reason, fiber optic coating has become attractive field for the fiber optic sensors. Most of these sensors are based on Fiber Bragg Grating (FBG). FBG type sensors can be used either as a direct sensing element or transducer. For example, polyvinyl alcohol (PVA) coated Fiber Bragg Grating which in the presence of high humidity the coated material's refractive index changes which can be measured (Dong et al. (2011), Yang et al. (2015), Venugopalan et al. (2008)). This is an example of transducing process. Consequently, temperature sensitivity (Park et al., 2011), humidity sensitivity (Wong et al., 2012), and acoustic sensitivity (Cusano et al., 2007) can be enhanced by coating fiber optic with novel polymers whose properties alter when the measurand has changed.

For optical films, we also require the material to be transparent at the wavelength of interest. The polyvinyl alcohol (PVA) is chosen since it is transparent at the wavelength of interest and it is widely known and used for film coating. In order to understand better the sensing process, one must know physical properties of the film such as thickness as it is pointed out in (Caucheteur et al., 2008), (Paladino et al., 2007), and (Mathew et al., 2013). One must select an optimum coating thickness to achieve the highest sensitivity. However, it is not easy to determine thickness exactly in the nano-micro scale. Nowadays there are some ways to determine thickness of the curvilinear surfaces such as conventional scanning electron microscopy (SEM), ellipsometry method (Lee and Chao, 2005), and using fiber optic probe (Buffone et al., 2013). We demonstrate that phase diffraction method might be used to determine thickness of the coated thin films on curved surfaces with high sensitivity, especially for the case of optical fiber.

5.1. Covered Polymer Thickness Sensing

Phase diffraction method is investigated theoretically in Chapter 3. In that case, coated optical fiber should be considered as three layer geometry.

The Equation (3.36) is fundamental equation for these kind of problems. By using it thickness of the coated thin film might be determined, provided that other parameters are well known.

5.1.1. Experimental Procedure

Experimental procedure was divided into two parts : Preparation of PVA/water solution and coating of fiber optic with that. The former one is a simple procedure that includes dissolving PVA in a water. PVA granules (dry) is mixed with water to form 15% PVA solution. This PVA/water mixing is stirred approximately $70\,^{\circ}\mathrm{C}$ with the help of magnetic stirrer for 10 hours to make sure it is dissolved completely. Thus the PVA/water solution is prepared to coat fiber optic as thin films.

There are number of techniques to coat fiber optic. Two of them are widely used: Electrostatic Self-Assembly (ESA) and Langmuir - Blodgett Technique (LBT) (James and Tatam, 2006). The main reason for the utilisation of ESA and LBT is their ability of controlling thickness at a molecular level. However, usage of either two is redundant, challenging and time-consuming. Hence we decided to use dip coating (DC) technique which is relatively easier. There is a trade-off in between simplicity of technique and reaching desired thickness. Dip coating technique is simply staged as dipping substrate in a solution, withdrawing the substrate with a constant speed, and waiting for solvent to evaporate (See Figure 5.1).

The thickness can be calculated by taking Landau-Levich equation into account theoretically (Haar, 1965). According to the Landau-Levich equation, physical parameters such as liquid viscosity, liquid surface tension, density, gravity, and withdrawal speed must be well known to calculate the thickness. Instead of obtaining information about the exact values of physical parameters which is a challenging process, using optical methods, one can determine the thickness of the sample which is withdrawn with constant speed.

Before the coating, surface of the fiber optic is cleaned using Isopropyl Alcohol and dried. Fiber optic is immersed into 15% PVA solution and drawn from the solution with the certain speed. This process should be repeated when thicker coating are required.

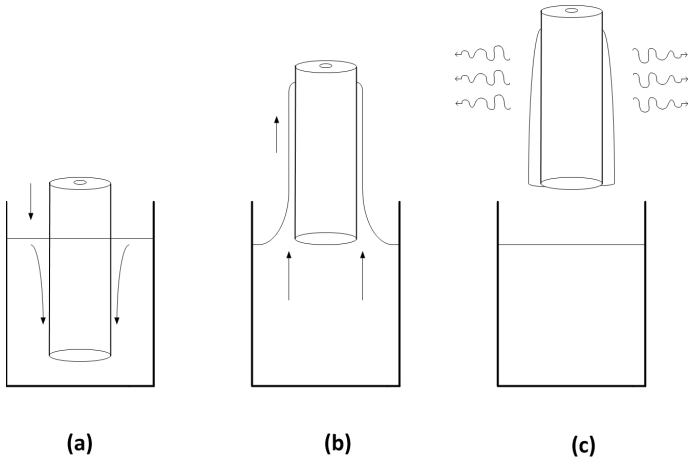

Figure 5.1. Dip coating process : (a) Immersing fiber optic into PVA solution (b) Withdrawing fiber optic with a constant speed (c) Waiting for solvent to evaporate

In order to achieve consistency for the withdrawn speed, we used simple electrical motor which has 18 revolutions per minute. Subsequently coated fiber optic is placed to an oven to make sure it is completely dried at $90\,^{\circ}\mathrm{C}$ for 2 hours. The dried PVA film is expected to have 1.53 refractive index as stated in both Gastón et al. (2004) and Alwis et al. (2013).

A schematic of the experimental setup is sketched in Figure 5.2. Experimental procedure begins with conversion of the output of the 632.8 nm He-Ne laser light beam to plane wave. Classical beam expander is used for this purpose. Obtained plane wave is sent through the PVA coated optical fiber perpendicular to its axis. The diffraction patterns are recorded by CCD camera whose distance from coated fiber optic is approximately 4.1 cm. Consequently, normalized intensity distributions on the Fresnel diffraction patterns are fitted the mathematical model by using least-squares method to extract value of the desired parameter.

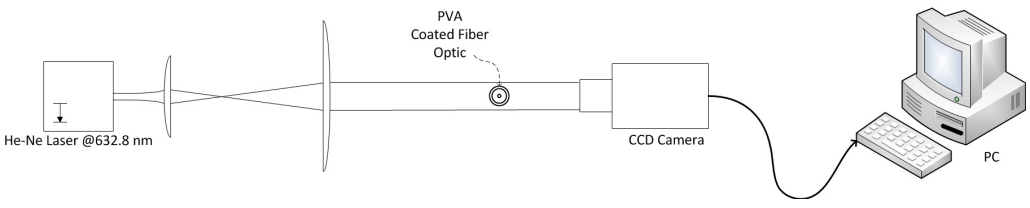

Figure 5.2. Top view of experimental setup for determining radius of the coated optical fiber

5.1.2. Results

In order to analyze the three samples and compare results to the our proposed technique, we took some Scanning Electron Microscope (SEM) images in Back-Scattered Electron Detector (BSED) mode to make sure it is coated. BSED simply responses dark or brighter in the sense of atomic number of area being analyzed. Thus, it is relatively easier to detect thickness. In order to analyze fiber optics by using SEM, fiber optics are broken, this is a destructive measurement method. These broken fiber optics can not be used again. However, here we offer non-destructive measurement method.

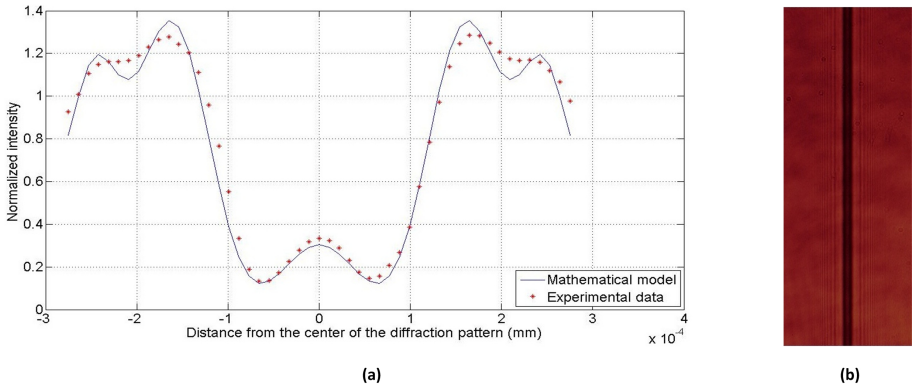

Figure 5.3. PVA coated optical fiber 1 : (a) The dots are normalized experimental intensity distribution , the curve is the theoretical intensity fitted c = 62940 nm (b) Diffraction pattern recorded by CCD of a laser beam diffracted by 440 nm PVA coated optical fiber

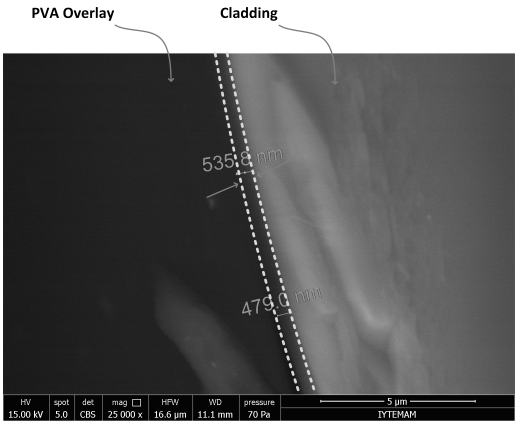

Figure 5.4. PVA coated optical fiber 1 SEM image in BSED mode reveals an overlay thickness of about 508nm

From Figures 5.3(a), 5.3(a) and 5.7(a), one can deduce the theoretical data and experimental data fits and 5.3(b), 5.3(b) and 5.7(b) demonstrate that CCD camera image that was taken from 4.1 cm distance from fiber optic approximately. The Figure 5.4 is the BSED image, brighter area indicates cladding of the fiber whereas dark area indicates PVA film. Additionally Figure 5.6(a) and Figure 5.8(a) are BSED images as well to show PVA films are coated smoothly.

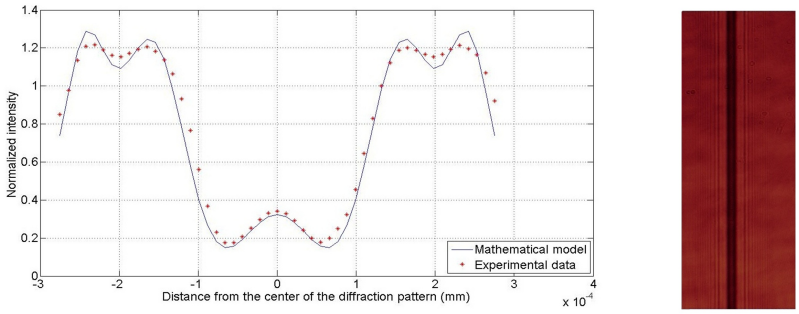

Figure 5.5. PVA coated optical fiber 2 : (a) The dots are normalized experimental intensity distribution, the curve is the theoretical intensity fitted c = 63429 nm (b) Diffraction pattern recorded by CCD camera of a laser beam diffracted by 929 nm PVA film coated optical fiber

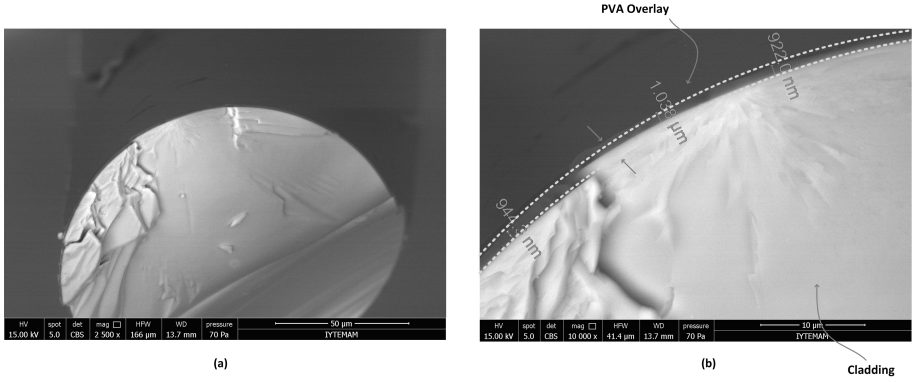

Figure 5.6. PVA coated optical fiber 2 SEM image in BSED mode (a) External view of 970 nm PVA film coated fiber optic (b) Thickness of the overlay is about 970 nm

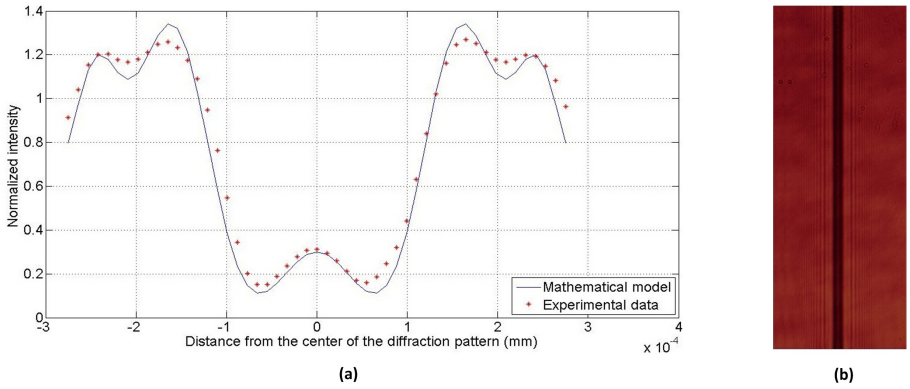

Figure 5.7. PVA coated optical fiber 3 : (a) The dots are normalized experimental intensity distribution, the curve is the theoretical intensity fitted c = 64130 nm (b) Diffraction pattern recorded by CCD camera of a laser beam diffracted by 1630 nm PVA film coated optical fiber

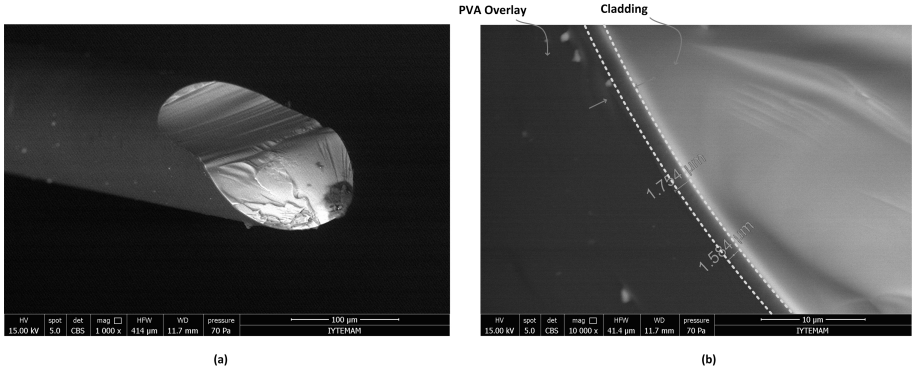

Figure 5.8. PVA coated optical fiber 3 SEM image in BSED mode (a) External view of 1670 nm PVA film coated fiber optic (b) Thickness of the overlay is about 1670 nm

Number	DC Process Repeating Time(s)	Thickness (nm) PD	Thickness (nm) SEM	Error (nm)	Radius error (%)
Fiber #1	1	440	508	68	13.3
Fiber #2	2	929	970	41	4.2
Fiber #3	3	1630	1670	40	2.3

Table 5.1. Summary of Coated Optical Fibers Thicknesses and Errors

CHAPTER 6

CONCLUSIONS AND FUTURE WORKS

In this thesis, diffraction effects from coated fiber optic is exploited to characterize coated thin dielectric film as it is aimed. Mathematical theory of diffraction is examined very carefully (Chapter 2). This examination is used to obtain mathematical model for our cases (Chapter 3). Although main research focuses on optical characterization of thin film coated fiber optic by using diffraction, we also show that diffraction from fiber optic can be used to determine surrounding refractive index, and take advantage of this sensitive technique to detect adulteration of olive oil. It is demonstrated that pure water's refractive index coincides, yet adulteration detection process does not match with the refractometer data due to temperature, wavelength dependency, and elapsed time between two measurements (Chapter 4). And finally, thin film thickness determination is done by comparing SEM results and experimental outputs. This process ends up with approximately 13.3%, 4.2%, and 2.3% radius errors for 508 nm, 970 nm, and 1670 nm respectively. In addition to that, it is a non-destructive measurement method which puts it one step forward (Chapter 5). On the other hand, optical characterization of adsorbent material (dielectric) coated on fiber optic can be considered as fiber optic sensor itself since optical properties of the material can be changed due to the surrounding medium effects (See Figure 6.1). For instance, thickness of the poly(methyl methacrylate) film is highly dependent on the ethanol level of the surrounding medium (Latino et al., 2012). The small changes of the ethanol in the gas-phase can be detected real time by using offered non-destructive method.

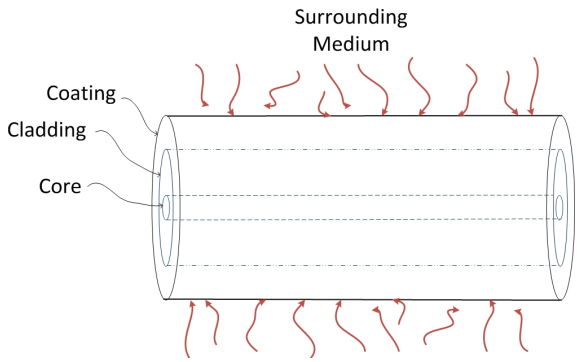

Figure 6.1. Typical optical fiber sensor coated with adsorbent material

There are still a lot to be done to further improvements in the sense of optical fiber sensor technology especially SPR based ones. Additionally, reactive near field techniques for diffraction integrals should be examined if diffraction limits are needed to be exceeded.

SPR based sensors as the name suggests exploit the ability of excitation surface plasmons that are the charge density oscillation of the free electrons in material, and propagating along the interface between materials whose dielectric constants signs are opposite, such as metal and dielectric. Their theoretical analysis is based on Maxwell's equations for evanescent fields. Transverse magnetic polarized incident waves excite the surface plasmons whereas transverse electric polarized waves are attenuated due to ohmic loss in the metal layer (Sharma et al., 2007). The formed electromagnetic field due to excitations decay exponentially into both media under a specific resonance condition. These all conditions related to excitation of surface plasmons introduce new concepts : SPR based fiber optics sensors. To enhance sensitivity cladding removed optical fibers or D-shaped cylindrical core optical fibers are used. Traditionally, fiber optics are coated with metals to excite surface plasmons. However, indium oxide which is a transparent conducting oxide was reported to better coating material than noble metals (Au and Ag)(Rani, 2014). Indium oxide has number of advantages such as, high transparency in the visible region, good electrical conductivity, and high IR reflectivity. Therefore, their characterizations especially thickness is crucial since its sensitivity highly related to thickness of the indium oxide (Rani et al., 2013). Phase diffraction methods might be used to determine its thickness.

Over the last few years, there is a growing interest for light scattering and diffraction from subwavelength structures where contribution from evanescent fields can not be ignored (Makris and Psaltis, 2011). Conventional scalar diffraction integrals fail to describe the process. As it is emphasized earlier section, our working region does not include reactive near field both experimentally and theoretically. We could not realize experimentally since it is challenging to reach that kind of thicknesses. From the theoretical point of view, it can be said that traditional scalar diffraction integrals must be modified by regarding oscillating dipoles instead of point sources to enable work on reactive (evanescent) near fields (Makris and Psaltis, 2011). Modified diffraction integrals can be examined whether these modified integrals yield more resolution since obtaining higher resolution beyond the limits that attract great deal of attention. In order to overcome this problem, there are lots of developments both reactive near and far fields nowadays. Reactive (evanescent) near field techniques exploit the fact that evanescent field carries information that can provide basis to exceed the limits. As modification diffraction inte-

grals takes evanescent fields into account, it might be considered as a candidate that can surpass the diffraction limits.

REFERENCES

Alwis, L., K. Bremer, T. Sun, and K. T. V. Grattan (2013). Analysis of the characteristics of pva-coated lpg-based sensors to coating thickness and changes in the external refractive index. *IEEE Sensors Journal 13*, 1117 – 1124.

Amiri, M. and M. T. M.Tavassoly (2006). Fresnel diffraction from 1d and 2d phase steps in reflection and transmission modes. *Optics Communications 272*, 349 – 361.

Angelis, M. D., S. D. Nicola, P. Ferraro, A. Finizio, and G. Pierattini (2000). Liquid refractometer based on interferometric fringe projection. *Optics Communications 175*, 315–321.

Ariponnammal, S. (2012). A novel method of using refractive index as a tool for finding the adultration of oils. *Research Journal of Recent Sciences 1*(7), 77–79.

Born, M. and E. Wolf (1999). *Principles of Optics* (7th ed.). Cambridge University Press.

Buffone, C., A. Glushchuk, C. S. Iorio, and F. Dubois (2013). Measurement of film thickness on a curved surface by fiber optic probe. *Journal of Electronics Cooling and Thermal Control 3*(1), 22–26.

Caucheteur, C., D. Paladino, P. Pilla, A. Cutolo, S. Campopiano, M. Giordano, A. Cusano, and P. Mégret (2008). External refractive index sensitivity of weakly tilted fiber bragg gratings with different coating thicknesses. *IEEE Sensors Journal 8*(7), 1330–1336.

Chen, Y. M. (1964). Diffraction by a smooth transparent object. *Journal Of Mathematical Physics 5*(6), 820–832.

Cusano, A., S. D'addio, A. Cutolo, S. Campopiano, M. Balbi, S. Balzarini, and M. Giordano (2007). Enhanced acoustic sensitivity in polymeric coated fiber bragg grating. *Sensors and Actuators B: Chemical 82*, 1450–1457.

Dong, X., T. Li, Y. Liu, Y. Li, C.-L. Zhao, and C. C. Chan (2011). Polyvinyl alcohol-coated hybrid fiber grating for relative humidity sensing. *Journal of Biomedical Optics 16*, 077001–077001–4.

Durán-Ramìrez, V. M., A. Martìnez-Rìos, J. A. Guerrero-Viramontes, J. Muñoz-Maciel, F. G. Peña-Lecona, R. Selvas-Aguilar, and G. Anzueto-Sánchez (2014). Measurement of the refractive index by using a rectangular cell with a fs-laser engraved diffraction grating inner wall. *Optics Express 22*(24), 29899–29906.

Faust, R. C. (1950). Fresnel diffraction at a transparent lamina. *Proceedings of the Physical Society. Section B 64*(2), 105–114.

Feynman, R. P., R. B. Leighton, and M. Sands (1965). *The Feynman Lectures on Physics*, Volume 3rd. Addison-Wesley.

Gastón, A., F. Pérez, and J. Sevilla (2004). Optical fiber relative-humidity sensor with polyvinyl alcohol film. *Applied Optics 43*, 4127–4132.

Ghatak, A. (2010). *Optics*. The McGraw-Hill Companies.

Golub, G. H. and J. H. Welsch (1969). Calculation of gauss quadrature rules. *Mathematics of Computation 23*(106), 221–230.

Goodman, J. W. (1996). *Introduction to Fourier Optics* (2nd ed.). The McGraw-Hill Companies.

Gurdeniz, G. and B. Ozen (2009). Detection of adulteration of extra-virgin olive oil by chemometric analysis of mid-infrared spectral data. *Food Chemistry 116*(2), 519–525.

Haar, D. T. (1965). *Collected Papers of L. D. Landau*. Intl Pub Distributor Inc.

Hecht, E. (2002). *Optics* (4th ed.). Pearson Education.

Huang, Y., B. Chen, G. Chen, and S. U. Khan (2013). Simultaneous detection of liquid level and refractive index with a long period fiber grating based sensor device. *Measurement Science and Technology 24*(9).

Huygens, C. (1690(1912)). Treatise on light : in which are explained the causes of that which occurs in reflexion, and in refraction, and particularly in the strange refraction of iceland spar.

James, S. W. and R. P. Tatam (2003). Optical fibre long-period grating sensors: characteristics and application. *Measurement Science and Technology 14*, 49–61.

James, S. W. and R. P. Tatam (2006). Fibre optic sensors with nano-structured coatings. *Journal of Optics A: Pure and Applied Optics 8*(7), 430–444.

Kao, K. C. and G. A. Hockham (1966). Dielectric-fibre surface waveguides for optical frequencies. *IEEE Proceedings 113*, 1151–1158.

Kedenburg, S., M. Vieweg, T. Gissibl, and H. Giessen (2012). Linear refractive index and absorption measurements of nonlinear optical liquids in the visible and near-infrared spectral region. *Optical Materials Express 2*, 1588–1611.

Latino, M., R. Montanini, N. Donato, and G. Neri (2012). Ethanol sensing properties of pmma-coated fiber bragg grating. *Procedia Engineering 47*, 1263–1266.

Laurie, D. P. (1997). Calculation of gauss-kronrod quadrature rules. *Mathematics of Computation 66*(219), 1133–1145.

Lee, K. Y. and Y. F. Chao (2005). The ellipsometric measurements of a curved surface. *Japanese Journal of Applied Physics 44*(32), 1015–1018.

Libish, T. M., M. C. Bobby, J. Linesh, S. Mathew, C. Pradeep, V. P. N. Nampoori, P. Biswas, S. Bandyopadhyay, K. Dasgupta, and P. Radhakrishnan (2013). Detection of adulteration in virgin olive oil using a fiber optic long period grating based sensor. *Laser Physics 23*(4).

Lu, S.-H., S.-P. Pan, T.-S. Liu, and C.-F. Kao (2007). Liquid refractometer based on immersion diffractometry. *Optics Express 15*(15), 9470–9475.

Makris, K. G. and D. Psaltis (2011). Huygens-fresnel diffraction and evanescent waves. *Optics Communications 284*, 1686–1689.

Mathew, J., Y. Semenova, and G. Farrell (2013). Effect of coating thickness on the sensitivity of a humidity sensor based on an agarose coated photonic crystal fiber interferometer. *Optics Express 21*(5), 6313–6320.

Mettler Toledo (2003). *Refractometers RE40D/RE50*. Mettler Toledo.

Miller, D. A. B. (1991). Huygen's wave propagation principle corrected. *Optics Letters 16*(18), 1370–1372.

Musso, M. D., R. Aschauer, A. Asenbaum, C. Vasi, and E. Wilhelm (2000). Interferometric determination of the refractive index of liquid sulphur dioxide. *Measurement Science and Technology 11*, 1714–1720.

Nufern (2013, 7). *Nufern 780 nm Select Cut-Off Single-Mode Fiber*. Nufern.

Paladino, D., A. Cusano, P. Pilla, S. Campopiano, C. Caucheteur, and P. Mégret (2007). Spectral behavior in nano-coated tilted fiber bragg gratings: Effect of thickness and external refractive index. *IEEE Photonics Technology Letters 19*(24), 2051–2053.

Park, C.-S., K.-I. Joo, S.-W. Kang, and H.-R. Kim (2011). A pdms-coated optical fiber bragg grating sensor for enhancing temperature sensitivity. *Journal of the Optical Society of Korea 15*(4), 329–334.

Raman, C. V. and I. Ramakrishna Rao (1926). Diffraction of light by a transparent lamina. *Proceedings of the Physical Society 39*(1), 453–457.

Rani, M. (2014). *Studies On Surface Plasmon Resonance Based Fiber Optic Sensors*. Ph. D. thesis, Jaypee Institute Of Information Technology.

Rani, M., N. K. Sharma, and V. Sajal (2013). Surface plasmon resonance based fiber optic sensor utilizing indium oxide. *Optik 124*(21), 5034–5038.

Renoirt, J.-M., C. Zhang, M. Debliquy, M.-G. Olivier, P. Mégret, and C. Caucheteur (2013). High-refractive-index transparent coatings enhance the optical fiber cladding modes refractometric sensitivity. *Optics Express 21*(23), 29073–29082.

Sabatyan, A. and M. T. Tavassoly (2007). Application of fresnel diffraction to nonde-

structive measurement of the refractive index of optical fibers. *Optical Engineering 46*, 128001–128001–7.

Sabatyan, A. and M. T. Tavassoly (2009). Determination of refractive indices of liquids by fresnel diffraction. *Optics and Laser Technology 41*, 892–896.

Saleh, B. E. A. and M. C. Teich (2007). *Fundamentals of Photonics* (2nd ed.). John Wiley and Sons.

Schot, S. H. (1992). Eighty years of sommerfeld's radiation condition. *Historia Mathematica 19*, 385–401.

Sharma, A. K., R. Jha, and B. D. Gupta (2007). Fiber-optic sensors based on surface plasmon resonance : A comprehensive review. *IEEE Sensors Journal 7*, 1118–1129.

Stratton, J. A. and L. J. Chu (1939). Diffraction theory of electromagnetic waves. *Physical Review 56*, 99–107.

Sun, X., W. Lin, X. Li, Q. Shen, and H. Luo (2015). Detection and quantification of extra virgin olive oil adulteration with edible oils by ft-ir spectroscopy and chemometrics. *Analytical Methods 7*(9), 3939–3945.

Sussman, M. H. (1962). Fresnel diffraction with phase objects. *American Journal of Physics 30*(2), 44–48.

Tavassoly, M. T., M. Amiri, E. Karimi, and H. R. Khalesifard (2005). Spectral modification by line singularity in fresnel diffraction from 1d phase step. *Optics Communications 255*, 23–34.

Tavassoly, M. T., R. R. Naraghi, A. Nahal, and K. Hassani (2012). High precision refractometry based on fresnel diffraction from phase plates. *Optics Letters 37*(8), 1493–1495.

Theimer, O., G. D. Wassermann, and E. Wolf (1952). On the foundation of the scalar diffraction theory of optical imaging. *Proceedings of the Royal Society of London. Series A, Mathematical and Physical 212*, 426–437.

Tsuda, H. and K. Urabe (2009). Characterization of long-period grating refractive index sensors and their applications. *Sensors 9*(6), 4559–4571.

Venugopalan, T., T. L. Yeo, T. Sun, and K. T. V. Grattan (2008). Lpg-based pva coated sensor for relative humidity measurement. *IEEE Sensors Journal 8*(7), 1093–1098.

Wojcik, A. B., M. J. Matthewson, K. T. Castelino, J. Wojcik, and A. Walewski (2006). Hybrid glass coatings for optical fibers: effect of coating thickness on strength and dynamic fatigue characteristics of silica fibers. In *Reliability of Optical Fiber Components, Devices, Systems, and Networks III*, Volume 6193. SPIE.

Wong, W. C., C. C. Chan, L. H. Chen, T. Li, K. X. Lee, and K. C. Leong (2012). Polyvinyl alcohol coated photonic crystal optical fiber sensor for humidity measurement. *Sensors and Actuators B: Chemical 174*, 563–569.

Yang, J., X. Dong, K. Ni, C. Chi Chu, and P. P. Shun (2015). Intensity-modulated relative humidity sensing with polyvinyl alcohol coating and optical fiber gratings. *Applied Optics 54*, 2620–2624.

Yang, M. and J. Dai (2012). Review on optical fiber sensors with sensitive thin films. *Photonic Sensors 2*(1), 14–28.

Yunus, W. M. M., Y. W. Fen, and L. M. Yee (2009). Refractive index and fourier transform infrared spectra of virgin coconut oil and virgin olive oil. *American Journal of Applied Sciences 6*(2), 328–331.

APPENDIX A

DERIVATIONS OF THE THEOREM AND THE CONDITION

A.1. Kirchhoff Integral Theorem

Here some important steps in the derivation of the integral theorem of Kirchhoff. This is relevant to discussion on page 9 (See Figure 2.2).

$$0 \;=\; \Big(\iint_S + \iint_{S_\epsilon}\Big)\Big\{\underbrace{\frac{\partial U}{\partial n}\Big(\frac{exp(jks)}{s}\Big) - U\frac{\partial}{\partial n}\Big(\frac{exp(jks)}{s}\Big)}_{\psi}\Big\}\,dS \tag{A.1}$$

$$\begin{aligned}
\iint_S \psi\, dS &= -\iint_{S_\epsilon}\Big\{\frac{\partial U}{\partial n}\Big(\frac{exp(jks)}{s}\Big) - U\frac{\partial}{\partial n}\Big(\frac{exp(jks)}{s}\Big)\Big\}\,dS \\
&= -\iint_{S_\epsilon}\Big\{\frac{\partial U}{\partial n}\Big(\frac{exp(jks)}{s}\Big) - U\Big(\frac{exp(jks)}{s}\Big)\Big(\frac{1}{s} - jk\Big)\Big\}\,dS \\
&= -\iint_{S_\omega}\Big\{\frac{\partial U}{\partial n}\Big(\frac{exp(jk\epsilon)}{\epsilon}\Big) - U\Big(\frac{exp(jk\epsilon)}{\epsilon}\Big)\Big(\frac{1}{\epsilon} - jk\Big)\Big\}\,\epsilon^2 d\omega \\
&= -\lim_{\epsilon\to 0}\iint_{S_\omega}\Big\{\frac{\partial U}{\partial n}\Big(\frac{exp(jk\epsilon)}{\epsilon}\Big) - U\Big(\frac{exp(jk\epsilon)}{\epsilon}\Big)\Big(\frac{1}{\epsilon} - jk\Big)\Big\}\,\epsilon^2 d\omega\,,
\end{aligned} \tag{A.2}$$

where $d\omega$ represents elements of solid angle. So as we take $\epsilon \to 0$ all the terms but second term goes to zero. The integration results $4\pi U(P)$ and it gives the Kirchhoff's integral theorem.

$$U(P) \;=\; \frac{1}{4\pi}\iint_S\Big[\frac{\partial U}{\partial n}\Big(\frac{exp(jks)}{s}\Big) - U\frac{\partial}{\partial n}\Big(\frac{exp(jks)}{s}\Big)\Big]\,dS. \tag{A.3}$$

A.2. Sommerfeld Radiation Condition

We discussed that there is no contribution from boundary $\mathbb{C}$ at infinity to the field intuitively, but the discussion was put on the mathematical basis by Sommerfeld.

$$\begin{aligned} U_{\mathbb{C}}(P) &= \frac{1}{4\pi} \iint_{\mathbb{C}} \frac{\partial U}{\partial n} \Big(\frac{exp(jks)}{s}\Big) - U \frac{\partial}{\partial n}\Big(\frac{exp(jks)}{s}\Big)\, dS \\ &= \frac{1}{4\pi} \iint_{\mathbb{C}} \frac{\partial U}{\partial n} \Big(\frac{exp(jkR)}{R}\Big) - U\Big(jk - \frac{1}{R}\Big)\Big(\frac{exp(jkR)}{R}\Big)\, dS \\ &= \frac{1}{4\pi} \iint_{\mathbb{C}} \Big(\frac{exp(jkR)}{R^2}\Big)\Big[\frac{\partial U}{\partial n} - jkU\Big] R\, dS + \iint_{\mathbb{C}} U\Big(\frac{exp(jkR)}{R^2}\Big) dS. \end{aligned} \tag{A.4}$$

Last integral on the RHS of the Equation (A.4) will vanish when we take the limit $R \to \infty$ due to the finiteness condition such that $|RU|$ remains bounded (Schot, 1992).

$$U_{\mathbb{C}}(P) \;=\; \frac{1}{4\pi} \iint_{\omega} \Big[\frac{\partial U}{\partial n} - jkU\Big] R\, d\omega, \tag{A.5}$$

where $d\omega$ again represents elements of solid angle. The integral will vanish to ensure there is no contribution from portion $\mathbb{C}$ if

$$\lim_{R\to\infty} R\Big[\frac{\partial U}{\partial n} - jkU\Big] = 0. \tag{A.6}$$

The Equation (A.6) is called Sommerfeld radiation condition. It guarantees that only outgoing waves satisfy.